NEUROSCIENCE

Reelin marks cocaine-activated striatal neurons, promotes neuronal excitability, and regulates cocaine reward

Kasey L. Brida[1], Emily T. Jorgensen[1], Robert A. Phillips III[1]†, Catherine E. Newman[1], Jennifer J. Tuscher[1]‡, Emily K. Morring[1], Morgan E. Zipperly[1]§, Lara Ianov[1,2], Kelsey D. Montgomery[3], Madhavi Tippani[3], Thomas M. Hyde[3,4,5], Kristen R. Maynard[3,4,6], Keri Martinowich[3,4,6,7], Jeremy J. Day[1]*

Drugs of abuse activate defined neuronal populations in reward structures such as the nucleus accumbens (NAc), which promote the enduring synaptic, circuit, and behavioral consequences of drug exposure. While the molecular and cellular effects arising from experience with drugs like cocaine are increasingly well understood, mechanisms that dictate NAc neuronal recruitment remain unknown. Here, we leveraged unbiased single-nucleus transcriptional profiling and targeted in situ detection to identify *Reln* (encoding the secreted glycoprotein, Reelin) as a marker of cocaine-activated neuronal populations within the rat NAc. A CRISPR interference approach enabling selective *Reln* knockdown in the adult NAc altered expression of calcium signaling genes, promoted a transcriptional trajectory consistent with loss of cocaine sensitivity, and decreased MSN excitability. Behaviorally, *Reln* knockdown prevented cocaine locomotor sensitization, abolished cocaine place preference memory, and decreased cocaine self-administration behavior. These results identify Reelin as a critical mechanistic link between neuronal activation and cocaine-induced behavioral adaptations.

INTRODUCTION

Reward-linked adaptive and learned behaviors are regulated by mesolimbic dopamine circuits in the brain (*1*–*4*). These circuits consist of dopaminergic neurons in the ventral tegmental area that densely innervate the nucleus accumbens (NAc), a subregion of the striatum that directly shapes motivated behaviors (*5*). Mesolimbic dopamine circuitry is a crucial target for many drugs of abuse (*3*), which act through distinct transporters, ion channels, and receptors to increase dopamine neurotransmission in the NAc (*6*, *7*). On short timescales, this increase in dopaminergic signaling promotes the excitability of medium spiny neurons (MSNs) in the NAc (*8*), leading to calcium influx and altered activity patterns (*9*–*11*). Over longer timescales (minutes to hours), dopamine receptor activation initiates well-defined signal transduction cascades that converge to regulate expression of immediate early gene (IEG) programs strongly linked to synaptic and behavioral plasticity (*12*–*16*). Together, these mechanisms serve as fundamental and conserved biochemical steps that link drug experience to the enduring molecular and physiological changes found in substance use disorders (*17*).

Despite the robust elevation in NAc dopamine produced by psychostimulant drugs like cocaine, emerging evidence suggests that cocaine experience activates a small proportion (~10 to 20%) of NAc neurons (*9*, *10*, *18*–*20*). Although small in number, these neuronal populations exhibit strong control over drug-related behaviors. Selective inactivation of neurons engaged by cocaine abolishes subsequent sensitized behavioral responses (*21*–*24*) and modulates cocaine seeking (*25*). While neuronal subtypes constituting drug-responsive populations vary based on drug class (*10*), cocaine preferentially affects dopamine receptor type 1 class MSNs [D1-MSNs; (*9*, *26*)], leading to increases in excitability (*8*, *27*, *28*), transcription of IEGs (*29*–*31*), and altered synaptic plasticity (*32*–*34*) that drives prolonged behavioral adaptations produced by drug exposure (*35*–*37*). However, even within the D1-MSN subpopulation, response to cocaine is highly heterogeneous (*9*), and the molecular mechanisms that determine participation of select neurons in drug response within the NAc remain unknown.

Here, we leveraged unbiased single-nucleus RNA sequencing (snRNA-seq) datasets collected after cocaine exposure (*20*, *38*) to identify markers of cocaine-activated D1-MSNs in the NAc. Unexpectedly, mRNA for the secreted extracellular matrix protein Reelin (encoded by the *Reln* gene) was enriched in D1-MSNs that were activated by cocaine. CRISPR-based knockdown of *Reln* decreased transcriptional states associated with activation by cocaine, altered expression of ion channels related to neuronal excitability, and impaired MSN excitability. Moreover, loss of *Reln* in the NAc abolished locomotor sensitization and place preference for cocaine and dampened cocaine self-administration behavior. Together, these results identify *Reln* as a stable marker of cocaine-sensitive neurons and reveal a key role for *Reln* in the transcriptional, electrophysiological, and behavioral properties of cocaine-induced striatal plasticity.

[1]Department of Neurobiology, University of Alabama at Birmingham, Birmingham, AL 35294, USA. [2]Civitan International Research Center, University of Alabama at Birmingham, Birmingham, AL 35294, USA. [3]Lieber Institute for Brain Development, Johns Hopkins Medical Campus, Baltimore, MD 21205, USA. [4]Department of Psychiatry and Behavioral Sciences, Johns Hopkins University School of Medicine, Baltimore, MD 21205, USA. [5]Department of Neurology, Johns Hopkins University School of Medicine, Baltimore, MD 21205, USA. [6]Department of Neuroscience, Johns Hopkins University School of Medicine, Baltimore, MD 21205, USA. [7]The Kavli Neuroscience Discovery Institute, Johns Hopkins University, Baltimore, MD 21205, USA.
*Corresponding author. Email: jjday@uab.edu
†Present address: Lieber Institute for Brain Development, Johns Hopkins Medical Campus, Baltimore, MD 21205, USA.
‡Present address: Department of Pharmacology and Toxicology, Medical College of Wisconsin, Milwaukee, WI, 53226, USA.
§Present address: Department of Psychiatry, University of Colorado Anschutz, Aurora, CO, 80045, USA.

RESULTS

Reln expression marks a cocaine-sensitive population of neurons in the NAc

Although cocaine promotes robust increases in dopamine capable of activating low-affinity DRD1 dopamine receptors on D1-MSNs, only a small fraction of D1-MSNs respond to cocaine as defined by increased calcium influx or IEG expression (*9*, *39*). This small population of activated neurons critically contributes to synaptic, cellular, and behavioral adaptations produced by cocaine (*9*, *21*, *26*). Despite the central role of these sparse populations, prior studies have not identified potential markers for this labile population that would predict drug responsivity. Previously, we identified a subpopulation of D1-MSNs within the NAc that exhibits a robust transcriptional response following acute and repeated cocaine exposure using snRNA-seq (*20*, *38*). Using these published datasets, we took an unbiased approach to identify a marker gene for the subset of cocaine-sensitive cells within this D1-MSN subtype (Fig. 1, A and B, and fig. S1A). We first subclustered all D1-MSNs to isolate the activated subpopulation from inactive populations (i1-i4; Fig. 1B). Activation was based on the average expression of significant cocaine differentially expressed genes (DEGs; Fig. 1G). Assessing differential transcript enrichment within the activated cluster, we identified *Reln* as a potential marker of this activated population (Fig. 1, C to F). More than 80% of activated D1-MSNs expressed *Reln* mRNA, with average expression ~10 times higher compared to inactive clusters (Fig. 1, D to F). *Reln* expression was also significantly correlated with composite IEG expression (Fig. 1F). When stratifying all D1-MSNs on the basis of *Reln* expression, only $Reln^+$ D1-MSNs demonstrated robust induction of IEGs, such as *Fos* (Fig. 1, G and H, and fig. S1). *Reln* levels were not altered by cocaine administration (Fig. 1I). These results were consistent when data were partitioned by acute or repeated exposure, although some IEGs exhibited exposure-dependent induction properties (fig. S2). Notably, cocaine-responsive D1-MSNs did not exhibit enrichment for *Creb1* mRNA (Fig. 1D), which encodes an activity-dependent transcription factor [adenosine 3′,5′-monophosphate response element–binding protein (CREB)] previously found to regulate memory engram (describing the group of ensembles engaged by cocaine) participation in other brain regions (*40*–*42*). Similarly, activation by cocaine was not predicted by expression of the *Drd1* dopamine receptor itself, which was consistently abundant across D1-MSN subclusters (Fig. 1D). While D1-MSNs are the principal neuronal population activated by cocaine, a small percentage of D2-MSNs also show increased IEGs. *Reln* similarly marks these cocaine-sensitive D2-MSNs, suggesting that it may serve as a broad marker of cocaine-sensitivity (fig. S3), although *Reln* does not mark activated neurons within *Reln*-enriched somatostatin or γ-aminobutyric acid (GABA)–undefined populations (fig. S4).

As cocaine-linked adaptations primarily depend on D1-MSNs, we focused on this population for in situ validation of *Reln* as a marker of cocaine-sensitivity using single-molecule RNA fluorescence in situ hybridization (smRNA-FISH). As in the acute snRNA-seq experiment, animals received a single intraperitoneal injection of either saline or cocaine (20 mg/kg) 1 hour before tissue collection. We then performed smRNA-FISH, probing for *Drd1*, *Reln*, and *Fos* (Fig. 1J) expression. Analysis was restricted to the NAc for direct comparison to snRNA-seq data. We observed a significant increase in Fos^+ cells in the cocaine group compared to that in the saline group (fig. S1C). As in the snRNA-seq data, $Reln^+/Drd1^+$ cells exhibited a significant increase in *Fos* expression compared to saline control, while $Reln^-/Drd1^+$ cells lacked this response (Fig. 1L). Similarly, *Reln* levels remained unchanged in D1-MSNs from rats treated with cocaine (Fig. 1M).

A parsimonious explanation for *Reln* enrichment in cocaine-activated MSNs is that *Reln* is either an activity-responsive IEG itself or is a direct target of transcription factors that are rapidly activated by cocaine. Notably, snRNA-seq (Fig. 1I) and smRNA-FISH (Fig. 1M) data both demonstrate that *Reln* expression is unaltered in D1-MSNs following cocaine experience, at the same time point where other IEGs are reliably detected. Additionally, reanalysis of prior work (*20*) revealed that *Reln* mRNA is not altered in primary striatal neurons following direct dopamine exposure (fig. S5), further suggesting that *Reln* is not an IEG. To investigate whether *Reln* may be a target of core transcription factors induced by cocaine and dopamine, we analyzed previously published datasets using a multiplexed CRISPR activation strategy to simultaneously overexpress key dopamine-induced transcription factors (*20*), including activator protein-1 (AP-1) factors (*Fos*, *Fosb*, and *Junb*), early growth response factors (*Egr2*, *Egr3*, and *Egr4*), and nuclear receptor subfamily 4 group A factors (*Nr4a1* and *Nr4a2*). Critically, *Reln* mRNA expression as detected by RNA sequencing (RNA-seq) remained unchanged following this manipulation (fig. S5). Together, these observations support the interpretation that *Reln* is a stable marker of D1-MSNs that are capable of actively participating in drug responses rather than a cocaine-responsive transcript.

Reln is enriched in D1-MSNs in both the rat and human brain and exhibits graded expression across the striatum

Although Reelin's roles in the cortex and hippocampus have been thoroughly studied (*43*–*46*), much less is known about its cellular and spatial distribution in the striatum. To further characterize the localization of *Reln* mRNA, we performed smRNA-FISH from rat coronal brain sections, probing for *Drd1*, *Drd2*, and *Reln*. Throughout the striatum, more $Drd1^+$ cells were also $Reln^+$ as compared to $Drd2^+$ cells, and $Drd1^+$ cells also expressed more *Reln* transcripts per cell (fig. S6B). This was also true of the NAc (Fig. 2, A and B). The striatum can be divided into anatomical subregions with different contributions to behavioral output (*47*, *48*). Therefore, we assessed *Reln* expression across striatal subregions [NAc core, NAc shell, ventrolateral striatum, ventromedial striatum, dorsolateral striatum (DLS), and dorsomedial striatum (DMS)]. This comparison revealed a gradient of $Reln^+$ cells, with a higher percent of $Reln^+$ cells in the dorsal striatum and nearly absent *Reln* expression in the NAc shell (fig. S6, C to G). This dorsal-ventral gradient of *Reln* expression is observed in both *Drd1* and *Drd2* neurons, although $Drd1^+/Reln^+$ cells outnumber $Drd2^+/Reln^+$ cells in every subregion except the shell (fig. S6C). As in the NAc as a whole, $Drd1^+$ cells expressed more *Reln* compared to $Drd2^+$ cells in the dorsal striatum (fig. S6D). *Reln* expression also exhibits lateralization, with more $Reln^+$ cells located in lateral subregions of the striatum as compared to medial subregions (fig. S6E). No sex differences in *Reln* expression were detected at either the anatomical or cellular level (fig. S6, H to K).

To examine expression of *Reln* in other species, we investigated publicly available data from the Allen Institute Mouse Brain Atlas and Human Brain Atlas (*49*, *50*). Both datasets confirmed enrichment of *Reln*/*RELN* mRNA expression in the adult striatum as compared to that in other brain nuclei (fig. S7) but lacked cell-type specificity in identification of *Reln*/*RELN* expression. Therefore, to determine whether *RELN* is also enriched in D1-MSNs in the human

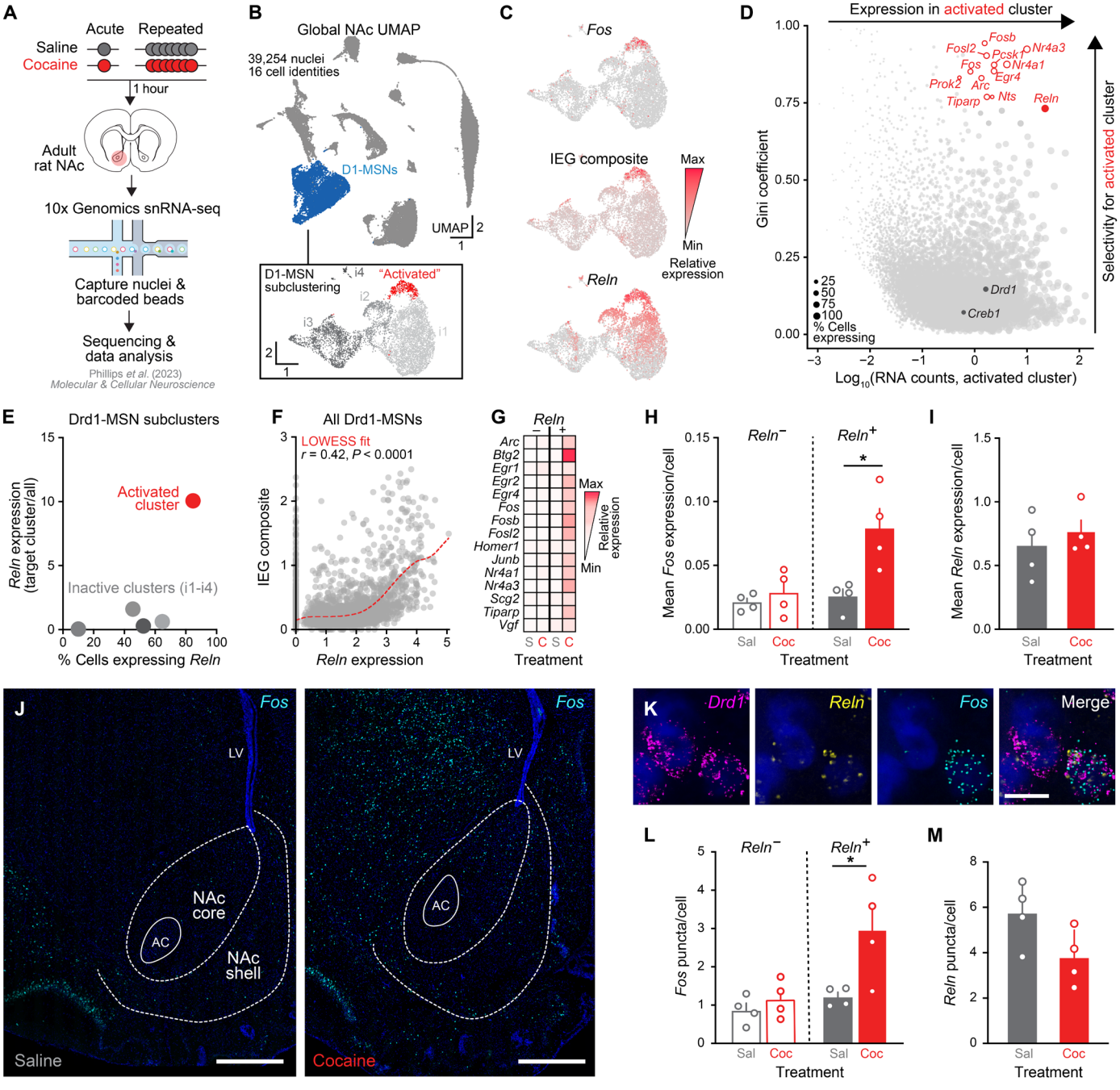

Fig. 1. *Reln* marks cocaine-sensitive *Drd1*$^+$ MSNs. (**A**) snRNA-seq workflow for acute and repeated saline or cocaine [data from (*38*)]. (**B**) Top: Uniform manifold approximation and projection (UMAP) of integrated NAc snRNA-seq. Bottom: Subclustered D1-MSNs (active, a1; inactive, i1-4). (**C**) Feature plots show *Fos*, other IEGs (composite expression), and *Reln* concentrated in subcluster a1. (**D**) Gini coefficient analysis identifies *Reln* mRNA as a selective and abundant marker of the a1 cluster (open circles, cocaine-responsive IEGs). (**E**) Percent of cells within a given cluster expressing *Reln* by cells' relative expression of *Reln* within a given cluster versus all other clusters. (**F**) *Reln* mRNA and composite IEG expression positively correlate (line, locally weighted scatterplot smoothing (LOWESS) fit). (**G**) Heatmap of IEG expression by treatment and *Reln* status. Data are mean values from all Drd1-MSNs, normalized to row average. (**H**) *Fos* levels in D1-MSNs by *Reln* expression and treatment. Only *Reln*$^+$ D1-MSNs demonstrate robust transcriptional response to cocaine [$P = 0.015$, nested one-way analysis of variance (ANOVA), Tukey's correction]. (**I**) Cocaine does not alter *Reln* expression (nested *t* test, $P = 0.49$). (**J**) Single-molecule RNA fluorescence in situ hybridization (smRNA-FISH) of *Fos* in saline animal (right) and cocaine animal (left; scale bar, 1 mm). (**K**) High-magnification NAc images from smRNA-FISH of *Drd1*, *Reln*, and *Fos* in cocaine-treated animal (scale bar, 10 μm). (**L**) *Fos* puncta in *Drd1*$^+$ cells by *Reln* expression. Only *Reln*$^+$ cells exhibit significant transcriptional response to cocaine ($P = 0.0433$, nested one-way ANOVA, Tukey's correction). (**M**) Cocaine does not alter *Reln* expression ($P = 0.08$, nested *t* test). *$P < 0.05$, **$P < 0.01$, ***$P < 0.001$, ****$P < 0.0001$. LV, lateral ventricle; AC, anterior commissure.

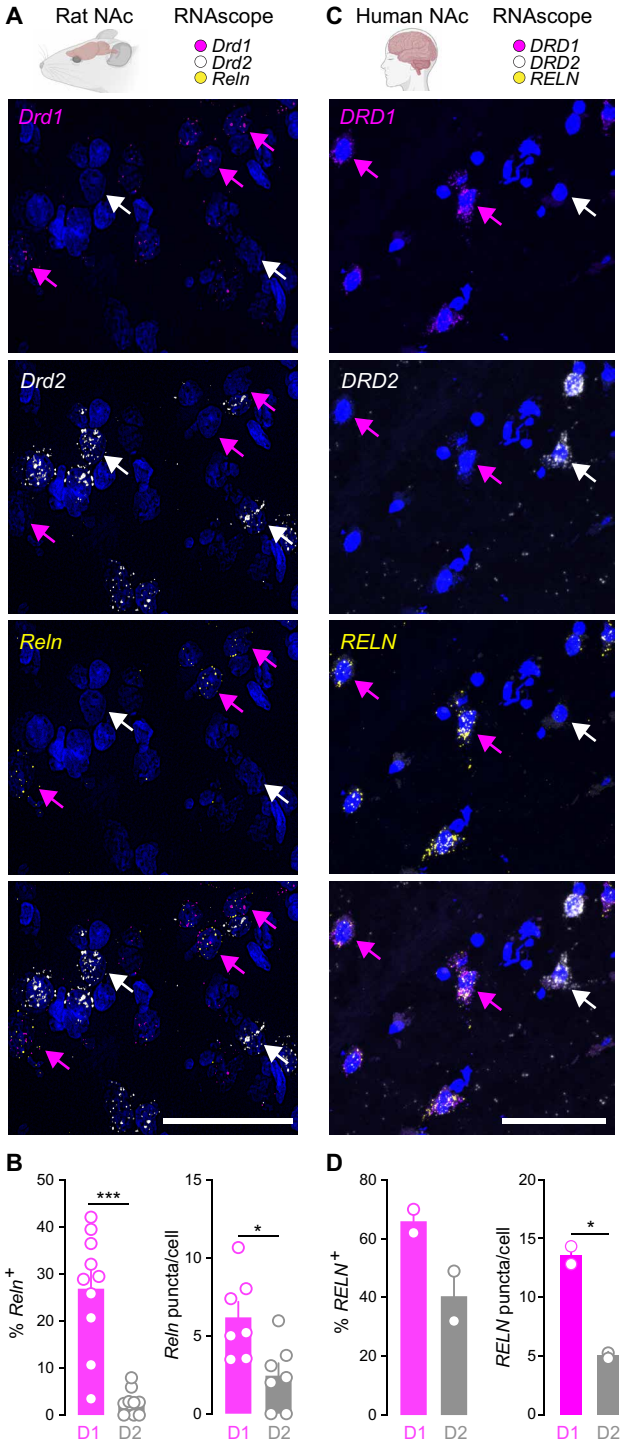

Fig. 2. Conserved enrichment of *Reln* mRNA in Drd1-MSNs in both rat and human NAc. (**A**) Multiplexed smRNA-FISH in NAc [blue, 4′,6-diamidino-2-phenylindole (DAPI); scale bar, 50 μm]. Magenta arrows indicate *Drd1*$^+$/*Reln*$^+$ cells, and white arrows indicate Drd2$^+$/Reln$^-$ cells. (**B**) Left: Percent of *Drd1*$^+$ and *Drd2*$^+$ cells that coexpress *Reln* mRNA (two-way ANOVA, interaction, $P < 0.0001$). Right: *Reln* mRNA puncta by cell type (paired *t* test, $P = 0.04$). (**C**) Multiplexed smRNA-FISH in human NAc (blue, DAPI; scale bar, 50 μm). Magenta arrows indicate *DRD1*$^+$/*RELN*$^+$ cells, and white arrows indicate DRD2$^+$/RELN$^-$ cells. (**D**) Left: Percent of *DRD1*$^+$ and *DRD2*$^+$ cells that coexpress *RELN* mRNA (paired *t* test, $P = 0.11$). Right: *RELN* expression by cell type (paired *t* test, $P = 0.04$). *$P < 0.05$, **$P < 0.01$, ***$P < 0.001$, ****$P < 0.0001$.

brain, we performed multiplexed smRNA-FISH in postmortem human NAc from two adult neurotypical donors for *RELN*, *DRD1*, and *DRD2*. In the human NAc, we found similar enrichment of *RELN* in *DRD1*$^+$ cells compared to that in *DRD2*$^+$ cells (Fig. 2, C and D). To further support this finding, we queried a publicly available snRNA-seq atlas of the human NAc from eight adult neurotypical donors and found similar enrichment of *RELN* mRNA in D1-MSNs (fig. S7D) (*51*). Collectively, these results highlight the enrichment of mRNA for Reelin in the adult striatum, reveal that it is expressed in the principal projection neurons of the striatum, and identify conserved enrichment in D1-MSNs across species.

CRISPR interference achieves targeted *Reln* knockdown in the NAc

While Reelin expression is high in the adult striatum and enriched in D1-MSNs (Fig. 2 and figs. S6 and S7) (*51*, *52*), the molecular and cellular roles of Reelin in this region are understudied. Thus, we sought to manipulate *Reln* expression in the NAc to identify its influences on MSN physiology and drug-related behaviors. Many prior investigations of *Reln* function have used the *Reeler* mouse model (*53*), in which a large genetic deletion causes loss of *Reln* expression (*45*). Similarly, mice harboring exon-skipping deletions that give rise to a truncated Reelin protein (*54*, *55*) have been used to model similar variants observed in a schizophrenia patient (*56*). However, given the germline nature of these transgenic mouse lines, the critical role Reelin plays in neurodevelopment, and the abundant expression of *Reln* outside the striatum (*43*, *44*, *57*), these models do not permit specific investigation of Reelin function in the NAc. To circumvent these confounds and enable post–developmental *Reln* manipulations in a rat model system, we developed a CRISPR interference (CRISPRi) strategy to achieve targeted *Reln* knockdown in the NAc. This CRISPRi system consists of a catalytically inactive (dead) *Streptococcus pyogenes* Cas9 (dCas9) fused to the transcriptional repressors Kruppel-associated box and Methyl CpG-binding protein 2 (KRAB-MeCP2) (*58*–*60*) and a guide RNA (gRNA) targeting the *Reln* promoter (Fig. 3, A and B). As a negative control, we used a gRNA targeting the bacterial *lacZ* gene delivered with the same dCas9-KRAB-MeCP2 CRISPRi machinery (Fig. 3, A and B). Both the *Reln* and *lacZ* gRNA vectors coexpress a fluorescent mCherry reporter, enabling visualization of transduction in live or fixed cells (Fig. 3C). Co-delivery of these constructs using lentiviruses led to robust knockdown of *Reln* mRNA and Reelin protein in primary striatal neurons (Fig. 3, D and E), mimicking heterozygous genetic deletions. To evaluate the specificity of this manipulation across the genome, we performed RNA-seq following *Reln* knockdown in rat primary striatal neurons (Fig. 3F and table S1). As expected, we observed significant down-regulation of *Reln* mRNA in neurons transduced with *Reln*-targeting CRISPRi machinery, and *Reln* was the top DEG both by effect size [$\log_2$(fold change) = −2.46] and statistical significance (adjusted *P* value = 0). Genes overlapping with computationally identified off-target sequence predictions (allowing for sequence mismatches and RNA or DNA bulges) were not consistently or robustly altered by *Reln* CRISPRi [|$\log_2$(fold change)| values < 0.5; Fig. 3F].

To assess in vivo efficacy of *Reln* CRISPRi in the NAc, we stereotaxically delivered lentiviruses expressing dCas9-KRAB-MeCP2 and *lacZ* gRNA to one NAc hemisphere and dCas9-KRAB-MeCP2 and *Reln* gRNA to the opposite NAc hemisphere (Fig. 3G). *Reln* knockdown was assessed using smRNA-FISH probing for *Reln*, *Cas9*, and

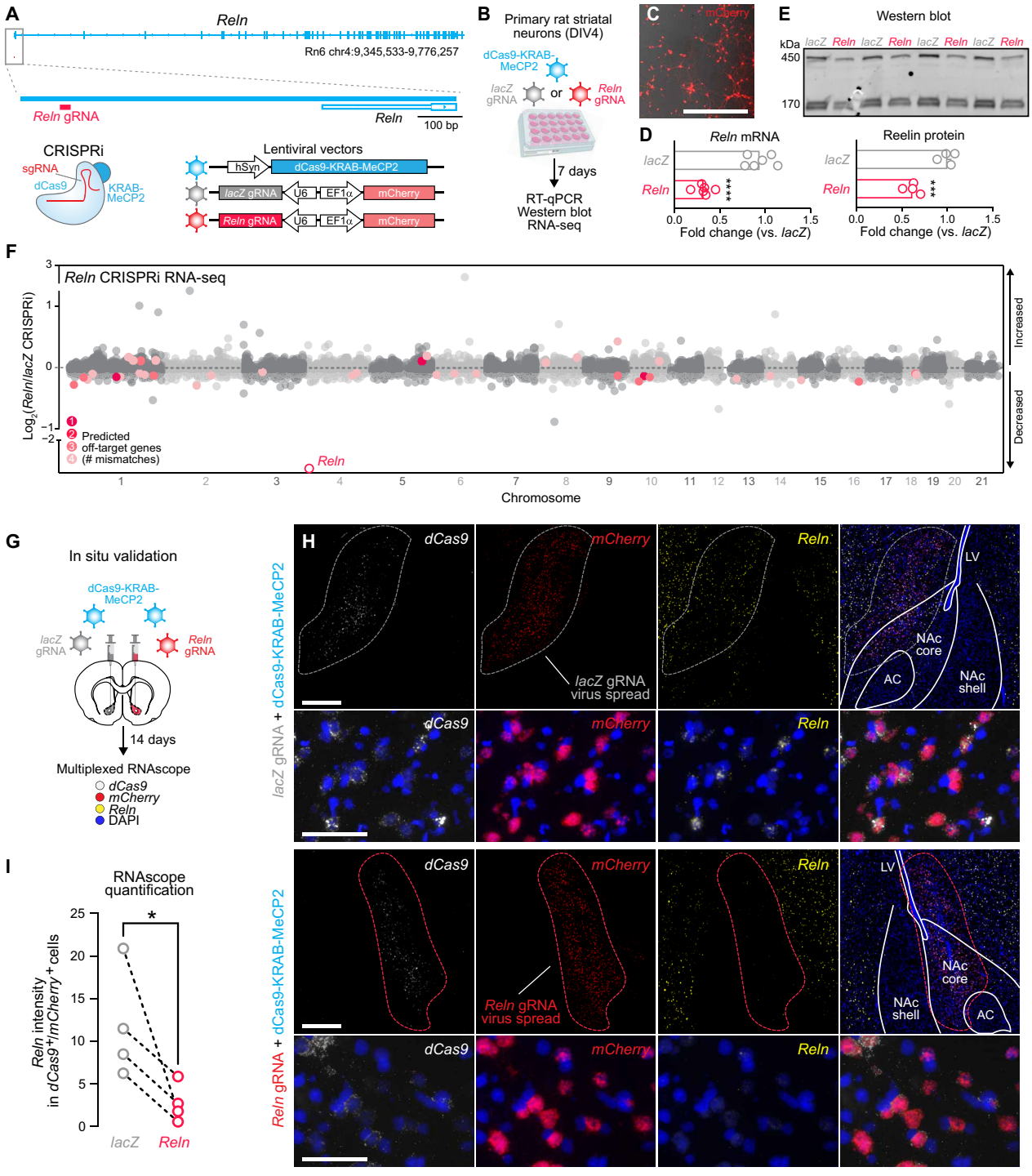

Fig. 3. Validation of CRISPR-mediated *Reln* knockdown. (**A**) Genomic location of CRISPRi *Reln* gRNA and schematic of CRISPRi lentiviral vectors for *Reln* or *lacZ* (control) targeting. (**B**) Timeline for lentiviral delivery in primary striatal neurons. (**C**) Representative image of transduction efficiency (mCherry reporter; scale bar, 10 μm). (**D**) CRISPRi at *Reln* robustly decreases *Reln* mRNA (RT-qPCR; $P < 0.0001$, nested *t* test). (**E**) Top: Western blot of secreted Reelin protein from neuronal culture media. Bottom: CRISPRi at *Reln* reduces total (450 kDa + 170 kDa) Reelin protein ($P < 0.001$, unpaired *t* test). (**F**) Manhattan plot highlighting significant Cas-OFFinder target predictions by number of mismatches in *Reln* CRISPRi primary striatal neuron bulk RNA-seq data reveals absence of off-target effects. (**G**) Schematic of in vivo validation for *Reln* CRISPRi followed by smRNA-FISH. *lacZ* gRNA + dCas9 was delivered into one hemisphere and *Reln* gRNA + dCas9 was delivered into the opposite hemisphere within a single animal. (**H**) Top: 40x-magnification images of the NAc (scale bar, 500 μm; dashed line indicates virus localization) of *lacZ* hemisphere. High-magnification images (scale bar, 50 μm) showing transcript puncta from *lacZ* hemisphere. Bottom: 40x-magnification images of the NAc (scale bar, 500 μm; dashed line indicates virus localization) of *Reln* hemisphere. High-magnification images (scale bar, 50 μm) showing transcript puncta from *Reln* hemisphere. (**I**) In vivo CRISPRi at *Reln* successfully decreases *Reln* expression (quantification within cells expressing both *dCas9* and *mCherry* mRNA; $P = 0.035$, ratio-paired *t* test). *$P < 0.05$, **$P < 0.01$, ***$P < 0.001$, ****$P < 0.0001$.

mCherry (to identify transduced cells; Fig. 3, H and I). Image analysis was restricted to the region of virus spread, and knockdown was quantified in cells coexpressing the gRNA and dCas9 constructs as cotransduction is necessary for knockdown. As with in vitro approaches, we detected significantly decreased *Reln* mRNA in cells targeted with CRISPRi machinery as compared to that in the *lacZ* control, confirming that *Reln* CRISPRi achieved robust in vivo knockdown (Fig. 3I).

Loss of *Reln* induces transcriptional alterations in NAc D1-MSNs

To better understand Reelin's role in the NAc, we performed snRNA-seq to identify transcriptional perturbations induced by *Reln* CRISPRi. Animals received bilateral infusions of dCas9-KRAB-MeCP2 in addition to either the *lacZ* or *Reln* gRNA. Two weeks later, NAc punches were obtained and prepped for snRNA-seq using the 10x Genomics platform as previously described (*20*). Clusters were benchmarked to our published snRNA-seq datasets from the NAc, with high agreement between the defined populations in this study and our previous work (fig. S8A). We detected no significant differences in marker gene expression between gRNA targets in neuronal populations (fig. S8A). Similarly, cell-type distribution did not differ on the basis of gel-bead in emulsion (GEM) well or treatment group (Fig. 4C). We detected *Reln* knockdown only in D1-MSNs in the *Reln* gRNA group compared to that in *lacZ* controls (Fig. 4D and fig. S8C) and focused subsequent analysis on this population given its selective activation by cocaine (*10*, *20*) (Fig. 1). DEGs identified using rigorous pseudobulked analysis (*61*) for all cell populations are noted in table S2. Within the D1-MSN cluster, we identified 28 DEGs (21 up-regulated and 7 down-regulated; Fig. 4E and table S2), with changes in

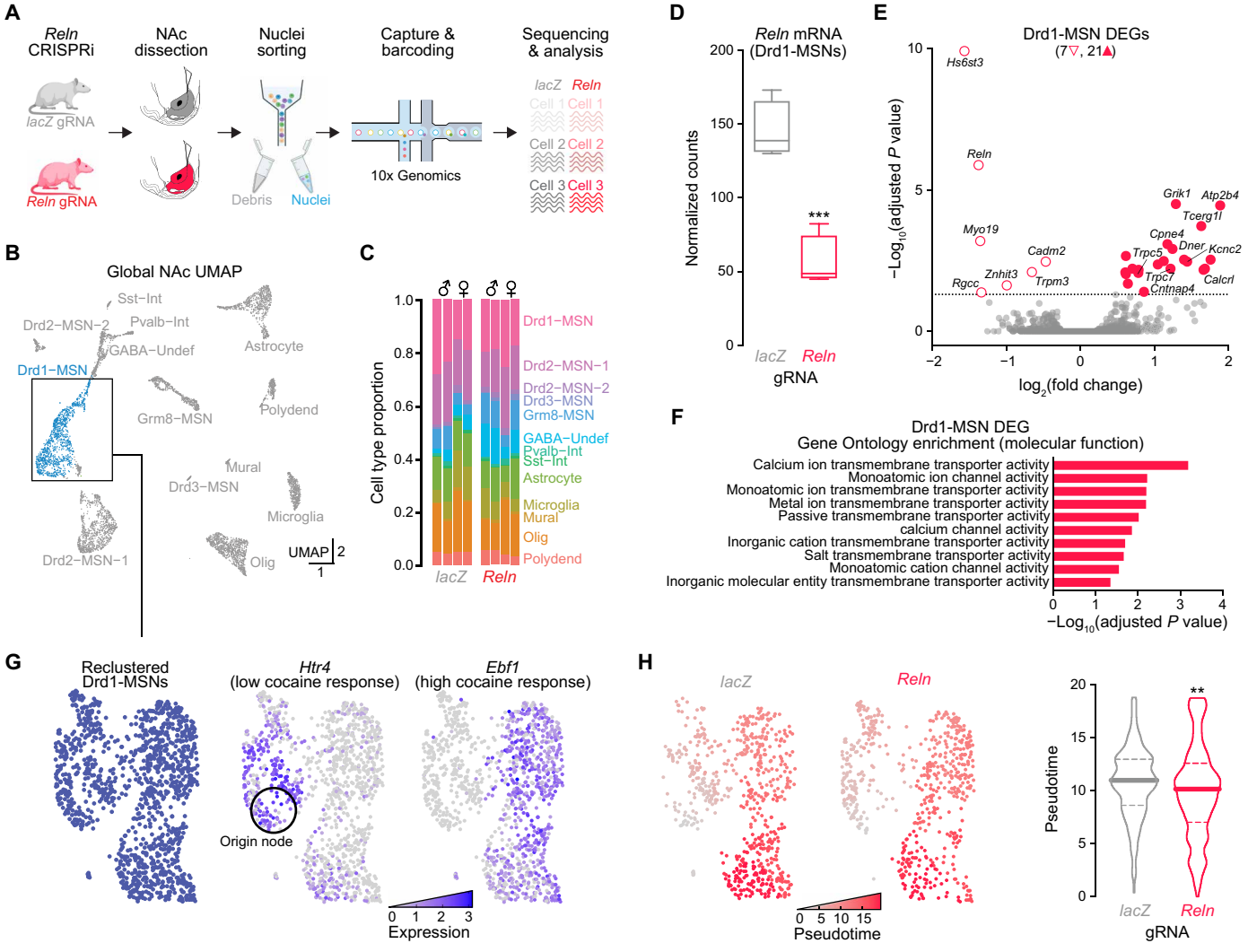

Fig. 4. *Reln* knockdown in the NAc alters expression of calcium channel genes. (**A**) snRNA-seq experimental schematic. (**B**) UMAP demonstrating presence of previously described transcriptional cell types within the NAc. (**C**) Cell-type proportions across defined clusters are not altered by *Reln* CRISPRi. (**D**) *Reln* levels are decreased in Drd1-MSNs in the *Reln* gRNA versus *lacZ* gRNA group ($P = 0.0005$, *t* test). (**E**) Volcano plot showing DEGs within the Drd1-MSN population. (**F**) Molecular function gene ontology analysis of Drd1-MSN DEGs highlights enrichment of genes involved in calcium ion channel and transporter functions. (**G**) Reclustering of Drd1-MSNs. High *Htr4* expression pocket set as origin node for pseudotime analysis. (**H**) Feature plot of Drd1-MSNs colored by pseudotime score (left), with higher scores representing cell states associated with activation by cocaine. Loss of *Reln* mRNA decreased pseudotime score (right; Kolmogorov-Smirnov test, $P = 0.0094$). $^{*}P < 0.05$, $^{**}P < 0.01$, $^{***}P < 0.001$, $^{****}P < 0.0001$.

several genes that function as calcium binding proteins (*Cpne4*), calcium-permeable channels (*Trpm3*, *Trpc5*, and *Trpc7*), and synaptic cell adhesion proteins (*Cadm2* and *Cntnap4*). Gene ontology analysis for molecular function categories revealed enrichment of terms related to ion channels, led by calcium transport and signaling (Fig. 4F).

In previous work, we demonstrated that an *Ebf1*$^+$ D1-MSN subpopulation exhibits transcriptional sensitivity to cocaine, whereas *Htr4*$^+$ D1-MSNs are not activated by cocaine (*38*). As *Reln* marks cocaine-sensitive D1-MSNs, we predicted that *Reln* knockdown would shift transcriptional profiles of D1-MSNs toward a more cocaine-insensitive state akin to *Htr4*$^+$ D1-MSNs. To assess this possibility, we performed pseudotime analysis with the *Htr4*$^+$ population set as the origin node (lowest pseudotime score or lightest color; Fig. 4, G and H). To avoid the confound of *Reln* expression defining cocaine-sensitive cells, *Reln* was removed from the expression matrix, and D1-MSNs were reclustered before running pseudotime (Fig. 4G). *Reln* knockdown led to a significant shift in the distribution of pseudotime values, with more cells having lower pseudotime values that define the putative cocaine-insensitive D1-MSN population (Fig. 4H). Together, these results suggest that Reelin may facilitate a cocaine-responsive state by influencing the balance of MSN ion channel expression.

Reln knockdown disrupts MSN intrinsic excitability

In addition to the induction of IEGs, cocaine also leads to persistent changes in MSN excitability (*8*, *28*). Given that *Reln* knockdown alters the expression of various ion channels (Fig. 4 and table S2), we hypothesized that Reelin regulates neuronal excitability to promote a cell state necessary for cocaine responsiveness. To test this hypothesis, we performed whole-cell patch-clamp electrophysiology in the NAc core following CRISPRi-mediated *Reln* knockdown (Fig. 5A). *Reln* knockdown had no effect on passive membrane (Fig. 5B) or action potential properties (fig. S9, A to E). To determine whether NAc-specific *Reln* knockdown affects MSN excitability, we constructed an input-output relationship using a current step protocol. *Reln* knockdown led to a marked decrease in intrinsic excitability, evident by the inability of MSNs to sustain firing across increasing current steps (Fig. 5, C and D). *Reln* knockdown cells also demonstrated a lower firing threshold during current steps (fig. S9F). Additionally, MSNs exhibit a characteristic ~200-ms first spike latency that was significantly shortened with *Reln* knockdown (Fig. 5E), further suggestive of altered ion channel function. Together, these results suggest that loss of *Reln* does not alter basal electrophysiological properties but reduces MSN intrinsic excitability.

Reln is required for cocaine-linked behavioral adaptations

Collectively, our results suggest that *Reln* marks cocaine-activated neurons and serves to promote the excitability of NAc MSNs. Given the importance of activated MSNs for cocaine-related behavioral adaptations, we next sought to determine whether *Reln* also contributes to the locomotor, rewarding, and reinforcing properties of cocaine. We began with a locomotor sensitization assay, a widely used paradigm in which repeated exposure to the same dose of cocaine produces an escalated locomotor response (*62*, *63*). Two weeks following bilateral knockdown of *Reln* in the NAc (or delivery of control *lacZ* gRNA), animals received 2 days of intraperitoneal (i.p.)

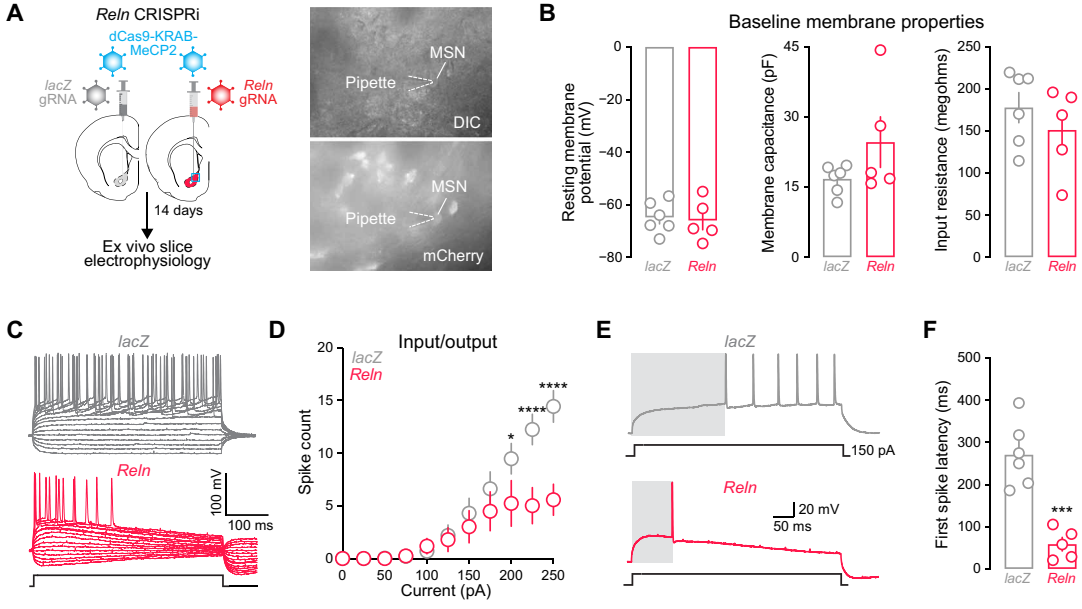

Fig. 5. *Reln* knockdown disrupts MSN excitability. (**A**) Left: Lentivirus delivery and experimental timeline. Right: Representative example of fluorescence-guided patch-clamp electrophysiology in the NAc. Top: Differential interference contrast (DIC) image with pipette and neuron labeled. Bottom: mCherry image showing pipette recording from neuron with mCherry fluorescence. (**B**) *Reln* knockdown did not alter passive properties such as resting membrane potential, membrane capacitance, or input resistance (*lacZ*, $n = 6$ animals, 17 cells; *Reln*, $n = 5$ animals, 11 cells; all $P > 0.05$, nested *t* test). (**C**) Representative traces across a current injection sweeps from a single representative cell from *lacZ* gRNA (gray) or *Reln* gRNA (red) recording. (**D**) Input-output curve from whole-cell patch-clamp electrophysiology in NAc comparing *Reln* knockdown cells to lacZ controls demonstrates significant attenuation of response to injected current, indicating lower intrinsic excitability (*lacZ*, $n = 6$ animals, 17 cells; *Reln*, $n = 5$ animals, 11 cells; $P < 0.001$, two-way ANOVA with Šidák multiple comparisons). (**E**) Representative traces highlighting difference in first spike latency [*lacZ* (top) and *Reln* (bottom)] at 150-pA current injection step. (**F**) *Reln* gRNA neurons exhibit shortened first spike latency [*Reln* average latency, 59.3 ms ($n = 5$ animals, 11 cells); *lacZ* average latency, 271.2 ms ($n = 6$ animals, 17 cells); $P = 0.0002$, nested *t* test]. *$P < 0.05$, **$P < 0.01$, ***$P < 0.001$, ****$P < 0.0001$.

saline injections, followed by two doses of cocaine [10 mg/kg, (ip)] separated by 1 week. We observed no differences in locomotion between *lacZ* gRNA and *Reln* gRNA animals during saline or initial cocaine exposure (fig. S10, A and B). While others have reported changes in anxiety-like behaviors in the setting of *Reln* deficiency (*64*, *65*), we found no differences in either center zone entries or time spent in center during open-field testing (fig. S10B), indicating that *Reln* knockdown in the NAc does not lead to anxiety-like behaviors. As expected, we observed robust cocaine locomotor sensitization in the *lacZ* gRNA group, with all animals increasing locomotor response to a second dose of cocaine (Fig. 6B). In contrast, *Reln* gRNA animals demonstrated a lack of sensitization to the second cocaine injection (Fig. 6B), suggesting that loss of *Reln* prevents neuronal adaptations linked to prior cocaine history.

While locomotor sensitization is frequently used as a behavioral correlate of cocaine-induced molecular and cellular plasticity, it does not directly measure cocaine reward or memory. To assess this facet of behavior, we used the cocaine conditioned place preference (CPP) paradigm (Fig. 6, A and C, and fig. S10, C to E). Two weeks following viral infusion of *Reln* CRISPRi vectors into the NAc, we performed an open-field assay and found no differences in baseline locomotion or anxiety-like behaviors, as in our locomotor sensitization cohorts (fig. S10, C and D). Next, we performed cocaine CPP pairings at doses of 10 and 20 mg/kg, each followed by a post-test session that enabled quantification of place preference. *Reln* CRISPRi produced lower preference for the cocaine-paired compartment, with an overall main effect of *Reln* gRNA and complete reversal of cocaine CPP at 20 mg/kg (Fig. 6C and fig. S10E). These results demonstrate that selective knockdown of *Reln* in the NAc alters reward-related behavior without affecting locomotion or anxiety-like behavior.

We next investigated whether effects of *Reln* knockdown extend to intravenous self-administration (IVSA), as drug context (i.e., experimenter administered versus self-administered) can affect the cellular and behavioral response to psychostimulants (*66*–*68*). Jugular vein catheterized animals received bilateral infusions of lentiviruses expressing dCas9-KRAB-MeCP2 and either *lacZ* or *Reln* gRNA 3 weeks before beginning cocaine IVSA acquisition and responding on a fixed ratio (FR) schedule (Fig. 6, A and D, and fig. S10E). Both groups exhibited

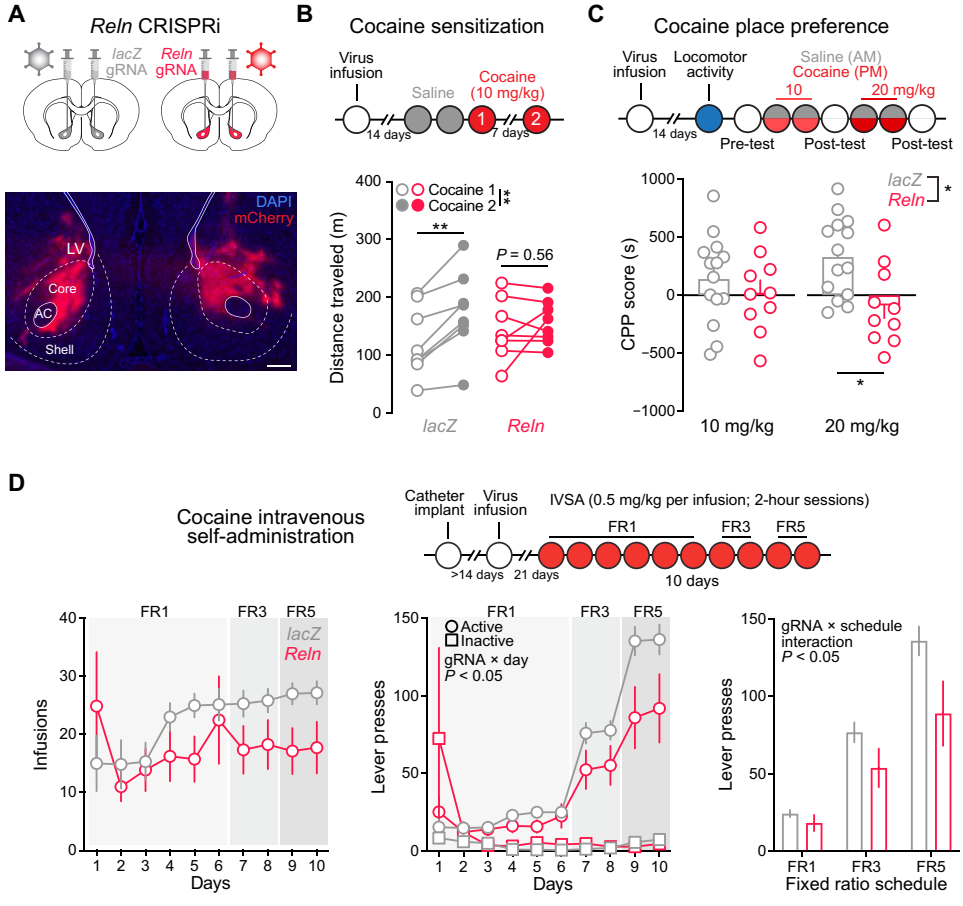

Fig. 6. *Reln* knockdown in the NAc impairs cocaine sensitization, CPP, and self-administration without altering locomotion. (**A**) Top: Schematic of bilateral lentiviral targeting. Bottom: Representative image showing expression of mCherry reporter (from gRNA lentivirus) in the NAc (scale bar, 500 μm). (**B**) *Reln* knockdown in the NAc prevents locomotor sensitization to cocaine (two-way repeated measures ANOVA; $P = 0.0465$ for gRNA x time interaction). (**C**) *Reln* knockdown abolishes CPP for cocaine (CPP score = time spent in cocaine paired chamber − time spent in saline paired chamber; two-way ANOVA with multiple comparisons and Tukey's correction; $P = 0.034$ for main effect of gRNA and $P = 0.014$ for effect of gRNA at 20 mg/kg). (**D**) Effects of *Reln* knockdown on cocaine IVSA infusions (left) and lever presses (center and right). Across days, *Reln* knockdown led to significantly fewer active lever presses (two-way ANOVA for active presses, $P = 0.0009$ for interaction between gRNA and days). *Reln* knockdown resulted in a schedule-dependent decrease in cocaine lever presses (two-way ANOVA, $P = 0.0472$ for interaction between gRNA and FR schedule). $^{*}P < 0.05$, $^{**}P < 0.01$, $^{***}P < 0.001$, $^{****}P < 0.0001$.

stable self-administration behavior, with expected sensitivity to changes in reinforcement schedule requirements (Fig. 6D). Control (*lacZ*) rats escalated cocaine infusions across behavioral training sessions [significant linear correlation between acquisition day and infusion number; coefficient of determination (R^2) = 0.295, $P < 0.0001$], whereas this correlation was absent in the *Reln* CRISPRi group ($R^2 = 0.0001$, $P = 0.907$). Additionally, loss of *Reln* decreased lever pressing behavior in a schedule-dependent way, with larger effects observed when increased effort was required for each cocaine infusion (Fig. 6D). Together, these results suggest that CRISPR-mediated *Reln* knockdown decreased the sensitizing, rewarding, and reinforcing properties of cocaine, without altering overall locomotion or initial locomotor response to cocaine.

Drugs of abuse and natural rewards engage distinct yet partially overlapping NAc populations (*18*, *69*). Thus, we next explored whether effects of *Reln* knockdown affect natural reward processes using a sucrose self-administration paradigm (fig. S11). Two weeks following bilateral viral infusions to the NAc (fig. S11), animals underwent sucrose self-administration following the same reinforcement schedules used for cocaine IVSA. To assess innate motivation for sucrose, animals were not food restricted for this experiment. Loss of Reelin did not decrease the number of sucrose rewards received or the number of active lever presses across this paradigm (fig. S11C), suggesting unique contributions of Reelin to drug reinforcement.

DISCUSSION

Drug-activated ensembles are key mediators of the cellular and behavioral effects of drug experience (*10*). The molecular changes that occur downstream of striatal neuron activation are increasingly well understood and include activation of signal transduction cascades; chromatin and transcriptional reprogramming; and coordinated alterations in expression of key receptors, neuropeptides, and ion channels (*17*, *20*, *70*–*74*). Despite these advances, determinants of drug ensemble participation have previously remained elusive. In this study, an unbiased approach identified *Reln* as a marker of cocaine-activated neurons in the NAc. While *Reln* is not altered after cocaine experience, it is abundantly expressed in NAc neurons expressing IEGs following cocaine administration, suggesting that *Reln* plays an active role in MSN excitability. To test this prediction, we developed a CRISPRi approach to repress *Reln* expression from the endogenous gene locus. NAc-specific loss of *Reln* disrupted transcriptional patterns in D1-MSNs, impaired intrinsic excitability of MSNs, and decreased cocaine-related behavioral adaptations. Together, these results establish *Reln* as both a marker and a regulator of cocaine-induced plasticity in the NAc.

In the developing brain, Reelin plays a central role in cortical layering (*44*, *45*) and segregation of the dopaminergic system (*75*, *76*). Postnatally, Reelin regulates synaptic function and long-term potentiation in the hippocampus through both posttranslational (*43*, *77*, *78*) and transcriptional mechanisms (*46*). Additionally, Reelin has links to diverse neuropsychiatric disorders, such as schizophrenia (*54*, *79*–*81*), substance use disorders (*82*, *83*), and Alzheimer's disease (*84*, *85*). Secreted Reelin protein is cleaved in the extracellular matrix by a variety of metalloproteases (*86*) and canonically acts at low-density lipoprotein receptors such as LRP8 (also known as ApoER2) and very-low density lipoprotein receptor (VLDLR) (*43*), although noncanonical modes of action have also been identified (*87*). Reelin binding at low-density lipoprotein receptors initiates cell signaling cascades largely mediated by the intracellular adapter protein, disabled-1 (DAB1), including phosphorylation of *N*-methyl-D-aspartate (NMDA) receptors by Src and Fyn family kinases and activation of the phosphatidylinositol 3-kinase–Akt–mammalian target of rapamycin pathway (*43*, *57*). Despite the presence of all of this machinery in the adult striatum and close links between Reelin and diseases arising from striatal dysfunction (*54*, *79*, *80*, *82*), few studies have explored Reelin's role in basic striatal biology. This lack of investigation likely stems from difficulties associated with measuring adult phenotypes in a model lacking a critical neurodevelopmental protein. Our CRISPRi approach avoids these developmental confounds and also enables site-specific reduction of *Reln* in the NAc.

Well-established models of Reelin function hold that, after the disappearance of Reelin-expressing Cajal-Retzius cells during neurodevelopment, Reelin levels are principally maintained by GABAergic interneurons (*43*). Therefore, the discovery that *Reln* mRNA marks projection neurons (MSNs) in the NAc that respond to cocaine was unexpected. However, this finding is in line with recent studies showing high expression of *Reln* in the murine dorsal and ventral striatum, as well as localization within MSNs (*52*, *88*, *89*). In agreement with our findings, these studies also identified *Reln* enrichment in $Drd1^+$ cells as compared to that in $Drd2^+$ cells in the mouse DMS (*52*) and higher expression in the NAc core versus shell (*88*). Our results build on these findings to characterize *Reln* expression throughout the entire striatum, confirming enrichment in $Drd1^+$ versus $Drd2^+$ populations across striatal subregions in the rat brain (fig. S6). We further define a dorsoventral and mediolateral gradient of *Reln* expression in the striatum, with the highest *Reln* levels in the DLS and near absence of *Reln* in the ventromedial NAc shell (fig. S6). Additionally, we validate the abundant expression of *RELN* mRNA in the human NAc and also reveal enrichment in $DRD1^+$ human neurons. These findings align closely with large scale transcriptional profiling studies of the human NAc (*51*) and highlight the translational relevance of *Reln* perturbations in animal models.

Our results define a previously undescribed role for Reelin in MSN physiology, with loss of *Reln* leading to a notable decrease in intrinsic excitability and altered expression of ion channels and calcium signaling proteins. This observation builds upon a strong body of literature supporting plasticity-promoting functions of Reelin in the hippocampus (*77*, *78*, *90*). Recent work in hippocampal neurons has also linked Reelin to neuronal excitability via NMDA-dependent regulation of calcium-permeable AMPA receptors (*91*). Similarly, synaptic Reelin signaling gates ketamine-induced plasticity in the hippocampus via maintenance of basal neurotransmission at the NMDA receptor (*92*). However, in the hippocampus, *Reln* mRNA is expressed by local interneurons and is absent in pyramidal neurons (*93*, *94*). Therefore, it is likely that the relationship between Reelin secretion and excitability in the striatum may be distinct from prior observations in the hippocampus, and future work will be required to comprehensively delineate these differences.

Rapid induction of IEGs such as *Fos* and *Arc* is a hallmark of electrical or synaptic activation across the nervous system (*95*–*97*). This relationship has been leveraged to generate a variety of widely used tools enabling permanent tagging and functional manipulations within neuronal ensembles (*98*–*101*). While the critical roles of various IEG transcription factors in plasticity of different brain circuits are increasingly appreciated (*71*, *102*–*104*), considerably less is known about the mechanisms that regulate ensemble participation.

Foundational work established that regulation of neuronal excitability by the activity-responsive transcription factor CREB served as a marker of activated neuronal ensembles (*40*–*42*, *105*, *106*). However, these studies all focused on activated ensembles in the amygdala, and similar markers of activated striatal ensembles have not been identified or functionally tested. The present results provide robust evidence from orthogonal and unbiased approaches that cocaine results in IEG transcription in a small population of *Reln*$^+$ neurons in the NAc.

The necessity of Reelin for cocaine sensitization, place preference, and self-administration supports the notion that cocaine sensitive-neurons are a primed population whose activation is crucial for diverse cocaine-related behavioral adaptations. Another interpretation of these findings is that *Reln* is important for basic neuronal functions that are also essential for cocaine-driven behavioral effects. However, given that *Reln* knockdown did not compromise passive properties of MSNs, baseline locomotion, or cocaine-induced locomotor responses, our results suggest that *Reln* regulates adaptive plasticity rather than basic aspects of neuronal function. These findings suggest that Reelin may participate in cocaine-related behaviors by acting as a mechanism that gates recruitment of individual NAc D1-MSNs into drug-activated ensembles, similar to CREB's role in the lateral amygdala where its sparse overexpression biases neuronal recruitment to cocaine ensembles (*42*). CREB's regulation of excitability might support this ensemble allocation bias as, within the hippocampus and amygdala, elevated excitability in the hours preceding contextual fear conditioning is positively correlated with the probability of subsequent recruitment into contextual fear ensembles (*105*, *107*). In this context, two possibilities arise regarding Reelin's role in ensemble allocation. First, Reelin may promote general cocaine sensitivity independent of cue or context associations, for example, simply by increasing intrinsic excitability of neurons that are subsequently activated by cocaine. Second, Reelin could regulate recruitment of association-specific neuronal ensembles, for example, by biasing responses to incoming glutamatergic inputs that convey information about environmental contexts or cues linked to cocaine experience (*108*, *109*). While Reelin has a well-defined role in regulating glutamatergic plasticity in the adult hippocampus (*77*, *78*, *91*, *92*, *110*), our finding that *Reln* marks ~80% of cocaine-activated neurons supports a role for Reelin in learning-independent regulation of general cocaine sensitivity as opposed to the learning-dependent selection of specific ensembles by drug-paired cues. It will be critical for future work to more thoroughly address these possibilities by characterizing the activation patterns of *Reln*$^+$ neurons across cocaine-related exposure and related learning, as well as via functional manipulation of *Reln*$^+$ neurons in operant or associative learning tasks.

While our findings provide a mechanistic link between Reelin expression and potential ensemble recruitment, it is unclear whether Reelin similarly marks activated neurons in other brain structures (or in response to other drugs of abuse or other rewarding stimuli). Ensemble participation is partially determined by drug class, with cocaine (a stimulant) primarily engaging D1-MSNs (*10*, *20*) and morphine (an opioid) recruiting both D1- and D2-MSNs (*10*, *111*). However, cocaine does activate a small group of D2-MSNs (*9*, *20*), and we similarly find enrichment of *Reln* mRNA in this MSN population (fig. S3). Thus, it is likely that *Reln* marks groups of activated neurons that span the boundaries between broad cell classes. While *Reln* knockdown does not decrease sucrose seeking behavior (fig. S11), this does not preclude the possibility that *Reln* marks cells that respond to other drugs of abuse. *Reln*'s role as a marker of cocaine-activated neurons appears specific to D1- and D2-MSNs, as activation of neurons in other *Reln* enriched populations is unrelated to *Reln* expression (fig. S4).

In addition to identifying *Reln* as a marker of cocaine-activated neurons, we report that loss of NAc *Reln* abolishes cocaine sensitization and place preference memory and decreases cocaine self-administration behavior. Prior studies investigating the role of Reelin in psychostimulant responses have generated mixed and often conflicting results. For example, haploinsufficient *Reeler* mice or mice harboring loss-of-function Reelin truncations exhibit decreased locomotor sensitivity to methamphetamine (*54*, *112*). However, *Reeler* mice display a normal locomotor response to amphetamine (*113*) and increased locomotor activity in response to cocaine, with intact cocaine CPP (*52*). Likewise, transgenic forebrain overexpression of *Reln* using the *Camk2a* promoter decreased cocaine locomotor sensitization without altering initial cocaine response (*79*). Given the strong developmental role of *Reln*, as well as its important functions in brain regions that send crucial projections to the NAc, these divergent results emphasize the need for continued exploration of Reelin's role in the adult striatum.

Defining *Reln* as a stable marker of cocaine-sensitive neurons may facilitate future efforts for a priori tagging, monitoring, and manipulation of this population. Together, these findings highlight an opportunity for high-precision manipulation of reward circuitry using *Reln*-based tools, reveal the necessity of Reelin in the cellular response to cocaine, and implicate the Reelin signaling pathway as a potential therapeutic target for cocaine use disorder.

MATERIALS AND METHODS

Animals

All animal model experiments were performed in accordance with the University of Alabama at Birmingham Institutional Animal Care and Use Committee (animal protocol no. 22245). Sprague-Dawley adult male and female rats (45 days old, patch-clamp experiments; 90 to 120 days old/225 to 250 g, all other experiments) were purchased from Charles River Laboratories (Wilmington, MA, USA). Rats were co-housed in pairs in plastic-filtered cages with wooden chewing block enrichment in an American Association for Accreditation of Laboratory Animal Care (AAALAC)-approved animal care facility maintained between 22° and 24°C on a 12-hour light/dark cycle with ad libitum access to food (Lab Diet SL3Z Irradiated rat chow) and water. Bedding and enrichment were changed weekly by animal resources program staff (no changes during behavioral testing as to not disturb animals). Animals were randomly assigned to experimental groups. All animals were handled by investigators for 5 to 7 days before behavioral testing.

Drugs

Cocaine hydrochloride (C5776, Sigma-Aldrich, St. Louis, MO, USA) was dissolved in sterile 0.9% sodium chloride and injected intraperitoneally at described doses (10 or 20 mg/kg) for cocaine CPP testing, cocaine locomotor response, and smRNA-FISH studies. For smRNA-FISH studies, cocaine was prepared as in behavioral testing at a dose of 20 mg/kg for intraperitoneal injections. For IVSA, cocaine was dissolved in sterile 0.9% sodium chloride for a final concentration of 2.5 mg/kg per milliliter (or 0.5 mg/ml per infusion). Two separate solutions were prepared for each sex on the basis of the

average weight of each sex. Cocaine solution was made fresh before behavioral testing and was protected from light.

Reln gRNA construction

The *Reln* gRNA was designed using an online single-guide RNA (sgRNA) tool, provided by the Zhang Lab at Massachusetts Institute of Technology (MIT) (crispr.mit.edu) and inserted in a previously described lentivirus compatible sgRNA scaffold construct. To ensure specificity, all CRISPR RNA (crRNA) sequences were analyzed with the National Center for Biotechnology Information's Basic Local Alignment Search Tool and Cas-OFFinder (www.rgenome.net/cas-offinder/).

Lentivirus production

Lentiviruses were produced in accordance with biosafety level 2 (BSL-2) safety guidelines in a biosafety cabinet, as previously described (*20*). For in vivo preparations, human embryonic kidney 293T cells were triple transfected with lentivirus packaging plasmid psPAX2 and the envelope plasmid pCMV-VSV-G (Addgene, plasmid nos. 12260 and 8454) in addition to the transgene of interest using FuGene HD (Promega). Medium was harvested at 48 and 72 hours post-transfection. Following harvest, medium was filtered (0.45 μm) and virus pelleted via ultracentrifugation (25,000 rpm, 1 hour and 45 min) and then resuspended in phosphate-buffered saline. Titers were obtained on freeze-thawed aliquots using the quantitative polymerase chain reaction (qPCR)–based TaKaRa lentivirus titration kit (no. 631235, Takara Bio, Kusatsu, Shiga, Japan). Minimum titers for all in vivo experiments were 1×10^{11} genome copies per milliliter. Virus was stored in single-use aliquots at −80°C. Before surgical infusion, viruses were thawed on wet ice and combined such that an equivalent number of genome copies for gRNA and effector made up the final mixture.

Stereotaxic surgery

Naïve adult male and female Sprague-Dawley rats (Charles River Laboratories) were anesthetized with 4 to 5% isoflurane and placed in a stereotaxic apparatus (Kopf instruments, Tujunca, CA, USA). Rats were maintained at a surgical plane of anesthesia with 2 to 3% isoflurane, and respiratory rates were monitored throughout surgery and maintained between 35 and 55 respirations per minute. Surgical coordinates were determined using the Paxinos and Watson rat brain atlas (sixth edition), targeting the NAc core bilaterally in *Reln* knockdown validation and behavioral studies and unilaterally for patch-clamp experiments. Under aseptic conditions, guide holes were drilled at anterior/posterior (AP) +1.7 mm, mediolateral (ML) ±1.5 mm, and the infusion needle was lowered to dorsal/ventral (DV) −7.2 mm [all coordinates with respect to bregma; (*114*)]. All infusions were made using a gastight 30-gauge stainless steel injection needle and 10-μl syringe (Hamilton Company, Reno, NV, USA). Lentivirus constructs were infused bilaterally at a rate of 0.25 μl/min using a syringe pump (Harvard Apparatus, Holliston, MA, USA), totaling 1.5 μl per hemisphere. Following each infusion, needles remained in place for 10 min to allow for diffusion of the virus. Infusion needles were slowly retracted and guide holes were filled with sterile bone wax. The surgical incision was closed with interrupted 6-0 monofilament nylon sutures (Covidien, Dublin, Ireland). At the end of surgery, rats were administered buprenorphine (0.03 mg/kg) and carprofen (5 mg/kg) for analgesia, and topical bacitracin (500 units) was applied to the incision site as a skin protectant and antimicrobial treatment. Animals were placed on a heating pad covered by a sterile drape to maintain body temperatures during surgery.

Cocaine injections

For in situ validation of *Reln* as a marker for cocaine-sensitive D1 neurons, animals ($n = 2$ per sex per group) received a homecage intraperitoneal injection of either cocaine (20 mg/kg) or saline. Animals were euthanized 1 hour following injection, and tissue was harvested for smRNA-FISH as described below. For published experiments involving snRNA-seq (*20*, *38*), cocaine (20 mg/kg; or saline control) was administered intraperitoneally immediately before placement in a 43 cm–by–43 cm plexiglass locomotor activity chamber (Med Associates Inc., St. Albans, VT, USA) to monitor cocaine-induced increases in locomotion for 30 min after injection. Animals were euthanized 1 hour following one injection (acute treatment) or 1 hour following the last of seven daily injections (repeated treatment), and tissue was harvested for snRNA-seq as previously described. All injections took place between 2:00 and 5:30 p.m., and sessions were counterbalanced by sex and treatment condition.

Locomotor sensitization

Two weeks following viral infusion surgeries, animals ($n = 4$ animals per sex per group) received intraperitoneal saline injections on days 1 and 2 immediately before locomotor testing in an open-field chamber for 30 min. On day 3, animals received cocaine (10 mg/kg, ip) (equivalent in volume to saline injections) before locomotor testing. One week later (day 10), animals received another cocaine injection (10 mg/kg, ip) followed by 30 min of locomotor testing. All locomotor activity was monitored in a 43 cm–by–43 cm plexiglass locomotor activity chamber (Med Associates Inc., St. Albans, VT, USA) with opaque white wall covering and an open top.

Baseline locomotor testing

Before CPP testing, baseline locomotor ($n = 4$ animals per sex per group) activity was monitored for 30 min as described for locomotor sensitization experiments.

CPP testing

CPP testing was completed in a three-chamber apparatus with guillotine-style doors (Med Associates Inc.) using previously established protocols with minor modifications (*74*). The two chambers used for conditioning measured ~27 cm by 21 cm by 22 cm: one with opaque black walls and stainless steel bar flooring, and the other with opaque white walls and metal stainless steel grid flooring. The conditioning chambers were separated from one another by manual guillotine-style doors and a central gray compartment with solid flooring, measuring 12 cm by 21 cm by 22 cm. All three chambers had clear perforated acrylic lids with centrally placed house lights. Each apparatus included a 16-channel infrared controller (Med Associates Inc.) to track rodent position, in conjunction with Med PC software (v4.1.49; Med Associates Inc.). CPP testing began 2 weeks following lentiviral infusion surgeries of CRISPRi machinery targeting the NAc core. Male and female rats [$n = 14$ *lacZ* (6 males and 8 females) and 10 *Reln* (6 males and 4 females)] were placed in the central compartment on the first day of testing (i.e., pretest) and were permitted to explore all three chambers of the CPP apparatus during a 30-min session. Days 2 and 3 of testing were conditioning days. In the morning sessions, rats were given an intraperitoneal injection of saline immediately before being placed in the initially

preferred chamber for the 30-min session. In the afternoon sessions, rats were given an intraperitoneal injection of cocaine (10 mg/kg) before placement in the other (initially non-preferred) chamber. A posttest for the dose of 10 mg/kg was performed on day 4, where animals had free access to all three chambers as in the pretest on day 1. Animals then went through 2 more pairing days (days 5 and 6) for cocaine (20 mg/kg) with the posttest on day 7.

Sucrose self-administration

Sucrose self-administration was completed in an operant conditioning box (Med Associates Inc.), measuring 29.5 cm by 23.5 cm by 27.3 cm with retractable response levers, a house light and fan, cue lights above each lever, and a sucrose pellet dispense located inside of a sound-attenuating chamber that surrounded the operant box. Sucrose self-administration began 2 weeks following bilateral intracranial infusions for CRISPRi lentiviruses targeting the NAc core [$n = 7$ *lacZ* (3 males and 4 females) and 7 *Reln* (4 males and 3 females)]. Sessions started using a computer-issued command, signaled by illumination of the house light, fan, and protraction of both inactive and active levers. Responses on the active lever resulted in illumination of a cue light above the lever and lever retraction for 0.5 s, as well as delivery of a sucrose pellet to a hopper located between the inactive and active levers. Responses on the inactive lever had no programmed consequences. All animals began on an FR1 schedule reinforcement for each sucrose pellet delivery, which was maintained for the first 6 days of sucrose self-administration. FR schedules were then increased to FR3 (for 2 days) and then FR5 (for 2 days). All sessions lasted for 2 hours or until 500 sucrose rewards were reached.

Cocaine IVSA

IVSA was completed in an operant conditioning box (Med Associates Inc.), measuring 29.5 cm by 23.5 cm by 27.3 cm with retractable response levers, a house light and fan, cue lights above each lever, and a syringe pump located outside of a sound-attenuating chamber that surrounded the operant box. Jugular vein catheterization surgeries were performed by the vendor (Charles River Laboratories) before arrival at the University of Alabama at Birmingham, and 22-gauge vascular access buttons (Instech, VABR1B/22) were used for intravenous access. Cocaine IVSA began 3 weeks following bilateral intracranial infusions for CRISPRi lentiviruses targeting the NAc core [$n = 6$ *lacZ* (2 males and 4 females) and 8 *Reln* (4 males and 4 females)]. Sessions started using a computer-issued command, signaled by illumination of the house light, fan, and protraction of both inactive and active levers. Responses on the active lever resulted in illumination of a cue light above the lever and lever retraction for 20 s, as well as drug infusion (infusion time of 2.5 s and infusion rate of 2.636 ml/min). Responses on the inactive lever had no programmed consequences. All animals began on an FR1 schedule reinforcement for each cocaine infusion (0.5 mg/kg per infusion), which was maintained for the first 6 days of IVSA. FR schedules were then increased to FR3 (for 2 days) and then FR5 (for 2 days). All sessions lasted for 2 hours or until 100 infusions were reached.

Tissue collection from adult rat NAc

Animals were rapidly decapitated using a guillotine (World Precision Instruments, Sarasota, FL, USA). Brain tissue was extracted and submerged in cold 2-methylbutane and chilled on dry ice for ~1 min. Flash-frozen brains were then removed from the 2-methylbutane, wrapped in aluminum foil, and placed on dry ice. Tissue was stored at −80°C and equilibrated to −20°C for at least 1 hour before sectioning at −18°C on a Leica CM 1850 cryostat (Deer Park, IL, USA) in 10-μm sections.

smRNA-FISH and image acquisition in fresh-frozen rat tissue

smRNA-FISH was performed (no. 323136, ACD Bio, Newark, CA, USA) to probe for *Reln*, *Drd1*, and *Fos* (*Fos* quantification) or *Reln*, *Drd1*, and *Drd2* (*Reln* characterization) or *Reln*, *mCherry*, and *dCas9* (*Reln* knockdown) following the manufacturer's protocol for fresh-frozen tissue, as previously described (*115*, *116*). Briefly, tissue was submerged in ice-cold 10% normal-buffered formalin for 15 min, then serially dehydrated with ethanol, and then treated with hydrogen peroxide, followed by protease IV digestion. Slides were incubated with a combination of 3 probes (characterization study: *Reln*, *Drd1*, and *Drd2*; *Fos* quantification: *Reln*, *Drd1*, and *Fos*; and *Reln* knockdown: *Reln*, *mCherry*, and *dCas9*; nos. 1048921-C4, 317031-C3, 315641, 403591-C2, 43120, and 519411-C2, ACD Bio, Newark, CA, USA) and stored overnight in a 5× saline-sodium citrate (SSC) buffer. Probes were fluorescently labeled with Opal Dyes (Akoya Biosciences, Marlborough, MA, USA; characterization: Opal 520 assigned to *Drd1*, Opal 570 assigned to *Reln*, and Opal 690 assigned to *Drd2*; *Fos* quantification: Opal 520 assigned to *Drd1*, Opal 570 assigned to *Fos*, and Opal 690 assigned to *Reln*; and *Reln* knockdown: Opal 520 assigned to *spCas9*, Opal 570 assigned to *mCherry*, and Opal 690 assigned to *Reln*; all dyes diluted 1:750). Sections were stained with 4′,6-diamidino-2-phenylindole (DAPI) and cover slipped with ProLong Glass Antifade Mountant (P36984, Thermo Fisher Scientific, Waltham MA, USA). All images were acquired on a Keyence-BZ800 microscope. Within an experiment, all images were acquired with the same acquisition settings for a given objective and channel. For *Reln* characterization studies, 20x-magnification images of one striatal hemisphere were obtained across eight animals. Images were stitched using Keyence Image Analyzer software. For *Reln* knockdown studies, 20x-magnification images were obtained of the whole striatum and stitched using the Keyence Image Analyzer Software. For *Fos* quantification studies, 40x-magnification images of one striatal hemisphere were obtained per animal and stitched using the Keyence Image Analyzer software. For regional analyses of stitched images, rat brain atlas overlays were applied to the stitched images and used to make regional crops in Adobe Photoshop (Paxinos and Watson, sixth edition). For puncta analysis in *Reln* characterization studies, 8 to 14 100x-magnification images per striatal subregion per animal were obtained. For *Fos* quantification studies, 100x-magnification images of the NAc were obtained and stitched using Keyence Image Analyzer. All 100x-magnification images were converted to Nikon (.nd2) file formats for puncta quantification.

Rat smRNA-FISH image analysis

Images were thresholded and masked in ImageJ. Thresholds were obtained by taking the average value of thresholds for each image in a given channel. DAPI regions of interest (ROIs) were created using the StarDist-2D plugin ("Versatile fluorescent nuclei") mode, probability score of 0.45, and overlap threshold of 0.20. These DAPI ROIs were then applied to the different channels corresponding to *Reln*, *Drd1*, *Drd2*, or *Fos*, which were converted to 8-bit images and thresholded on the basis of an averaged auto-threshold value specific for each channel. Positivity was identified on the basis of mean intensity for each channel in the DAPI ROIs. Data were further processed using R to identify signal overlap for individual DAPI ROIs to identify

cell types. For *Reln* knockdown quantification, *Reln* intensity scores were used to quantify *Reln* expression in cells that coexpressed *mCherry* (gRNA) and *dCas9*. For puncta analysis, thresholds were defined in QuPath v0.3.2 (*117*) and held consistent for each channel across regions and animals. In downstream analyses, *K*-means clustering was used to identify relevant threshold values for puncta counts. R was again used to identify cell types based on the overlap of puncta within a given nuclear ROI.

Postmortem human tissue samples

Postmortem human brain tissue from two neurotypical adult donors was obtained at the time of autopsy through the Office of the Chief Medical Examiner of the State of Maryland following informed consent from legal next of kin, under the Maryland Department of Health Institutional Review Board protocol no. 12-24. Clinical characterization, diagnoses, and macro- and microscopic neuropathological examinations were performed on all samples using a standardized paradigm, and subjects with evidence of macro- or microscopic neuropathology were excluded. Details of tissue acquisition, handling, processing, dissection, clinical characterization, diagnoses, neuropathological examinations, RNA extraction, and quality control measures have been described previously (*118*). The NAc was dissected using a handheld dental drill at a level where the caudate and putamen are joined by the accumbens at the ventral aspect of the striatum, with clear striations separating the putamen from the caudate. The anterior aspect of the temporal lobe and the claustrum served as additional landmarks.

smRNA-FISH and image acquisition in postmortem human tissue

Two blocks of fresh frozen NAc from neurotypical control individuals were sectioned at 10 μm and stored at −80°C. For postmortem human studies (Fig. 2, C and D), in situ hybridization assays were performed with RNAscope technology using the RNAscope Fluorescent Multiplex Kit V2 and 4-plex Ancillary Kit (catalog nos. 323100 and 323120, Advanced Cell Diagnostics Bio-Techne, Hayward, CA, USA) according to the manufacturer's instructions. Briefly, tissue sections were fixed with a 10% neutral buffered formalin solution (catalog no. HT501128, Sigma-Aldrich, St. Louis, MO, USA) for 30 min at room temperature, series dehydrated in ethanol, pretreated with hydrogen peroxide for 10 min at RT, and treated with protease IV for 30 min. Sections were incubated with probes for *RELN*, *DRD1*, and *DRD2* (catalog nos. 413051-C2, 553991-C3, and 524991-C4, ACD, Hayward, CA, USA) and stored overnight in 4× SSC buffer. Probes were fluorescently labeled with Opal Dyes (Perkin Elmer, Waltham, MA; Opal570 diluted at 1:1500 and assigned to RELN, Opal690 diluted at 1:500 and assigned to DRD2, and Opal620 diluted at 1:500 and assigned to *DRD1*) and stained with DAPI to label the nucleus. Images were acquired in *z*-series using a Zeiss LSM780 confocal microscope as previously described (*119*).

Human smRNA-FISH image analysis

Automated image processing was performed using the dotdotdot MATLAB-based command line toolbox (*119*), which is available at https://github.com/LieberInstitute/dotdotdot. Downstream analyses were performed using R v4.0.0+2020.04.24.

Neuronal cell cultures

Primary rat striatal cell cultures were generated from E18 striatal tissue as described previously (*20*, *58*, *73*). Cell culture plates (Denville Scientific Inc., Plainfield, NJ, USA) were coated overnight with poly-L-lysine (50 μg/ml; Sigma-Aldrich), supplemented with laminin (7.5 μg/ml; Sigma-Aldrich), and rinsed with diH_2O. Dissected striatal tissue was incubated with papain (LK003178, Worthington Biochemical Corporation, Lakewood, NJ, USA) for 25 min at 37°C. After rinsing in complete Neurobasal media (supplemented with B27 and L-glutamine, Invitrogen), a single-cell suspension was prepared by sequential trituration through large to small fire-polished Pasteur pipettes and filtered through a 100-μm cell strainer (Thermo Fisher Scientific, Waltham, MA, USA). Cells were pelleted, resuspended in fresh medium, counted, and seeded to a density of 225,000 cells per well on 12-well culture plates (65,000 cells/cm^2). Cells were grown in complete neurobasal medium for 19 days in vitro (DIV19) in a humidified CO_2 (5%) incubator at 37°C with half-medium changes at DIV1, DIV4, DIV8, DIV13, and DIV16.

RNA extraction and qPCR

RNA was extracted per manufacturer's instructions using the QIAGEN RNeasy RNA extraction kit (no. 74106, QIAGEN, Hilden, Germany). cDNA libraries were synthesized using iScript Supermix (Bio-Rad). Expression of *Gapdh* (forward, ACCTTTCATGCTGGGGCTGGC; and reverse, GGGCTGAGTTGGGATGGGGAC) and *Reln* (forward, AATCGGCAAGAGTCACCGAAGCC; and reverse, CTGTCTGTGCCGTGCTCCCAA) were measured using reverse transcription (RT)–qPCR with the SYBR Green detection.

Bulk RNA-seq

Primary rat striatal neurons were transduced with lentiviruses expressing CRISPRi machinery on DIV12 with a multiplicity of infection per cell of 2000 for each virus. Primary neurons were harvested 1 week later on DIV19 after which RNA was extracted (RNeasy, QIAGEN) and submitted to the Genomics Core Lab at the Heflin Center for Genomic Sciences at the University of Alabama at Birmingham for library preparation. Four biological replicates were used per gRNA. Paired-end libraries (100 base pairs) were sequenced on an Illumina NovaSeq 6000 instrument. Raw FASTQ files were processed using nf-core/rnaseq v3.10 (https://doi.org/10.5281/zenodo.1400710) of the nf-core collection of workflows (*120*) using a pipeline executed with Nextflow v23.04.1 (*121*). Splice-aware alignment to the mRatBn7.2/Rn7 genome assembly was conducted using STAR v2.7.9a (*122*) with the associated Ensembl gene transfer format (gtf) file (version 105). Binary alignment map files were indexed with SAMtools (*123*) (v1.16.1). Gene-level counts were generated using featureCounts [Rsubread, v2.0.1; (*124*)]. Quality-control metrics were collected and reviewed with MultiQC (v1.13) (*125*), and a minimum of 20 million mapped reads were obtained per sample (range, 22.6 million to 121.4 million). Differential expression testing was conducted using DESeq2 (*126*) (v1.38.3). DEG testing *P* values were adjusted with the Benjamini-Hochberg method (*127*), and DEGs were designated as those genes with an adjusted P value < 0.05. Genes with unreliable/low expression estimates (base mean < 50) were excluded from subsequent analysis.

Off-target detection for CRISPRi

Potential off-target sites for CRISPRi were identified using Cas-OFFinder (*128*), allowing up to two DNA or RNA bulges and up to four mismatches. Overlap between DEGs and Cas-OFFinder hits were assessed using the IRanges and GenomicAlignments tools with findOverlap() function (*129*). Manhattan plot highlighting lack

of off-target effects was generated in RStudio using the Manhattan package available at https://github.com/boxiangliu/manhattan/.

Western blot

Medium was harvested from rat primary striatal neuron cultures on DIV19, 7 days following transduction with lentiviruses expressing CRISPRi machinery to target *lacZ* or *Reln*. Medium (50 μl) was reduced and denatured before gel electrophoresis on a 4 to 15% tris-glycine gel (no. 4561084, Bio-Rad Laboratories, Hercules, CA, USA) for 2 hours at 175 mV. Protein was transferred to a polyvinylidene difluoride membrane at 4°C for 16 hours at 100 mV. Membranes were incubated in monoclonal Reelin antibody (Millipore, catalog no. MAB5364, RRID:AB_2179313) overnight at 4° before incubation with secondary for 2 hours (no. 926-68072, Li-Cor Biosciences, Lincoln, NE, USA) at RT. Blots were imaged on a Li-Cor Odyssey 9120. Protein was quantified in ImageJ using the gel analyzer tool to obtain area under the curve.

Whole-cell patch-clamp electrophysiology

To examine the role of Reelin in intrinsic excitability, whole-cell patch-clamp recordings were conducted as previously described (*130*). Sixty- to 120-day-old rats were briefly anesthetized with isoflurane and intracardially perfused with oxygenated ice cold recovery solution: 93 mM *N*-methyl-D-glucamine, 2.5 mM KCl, 1.2 mM NaH_2PO_4, 30 mM $NaHCO_3$, 20 mM Hepes, 25 mM glucose, 4 mM sodium ascorbate, 2 mM thiourea, 3 mM sodium pyruvate, 10 mM $MgSO_4(H_2O)_7$, 0.5 mM $CaCl_2(H_2O_2)$, and HCl added until pH was 7.3 to 7.4 with an osmolarity of 300 to 310 mosmol. Coronal slices (300 μm) were prepared on a vibratome (Leica VT1200S) containing recovery solution and then transferred to a Brain Slice Keeper (Automate Scientific) containing a holding solution for at least 1 hour before recording: 92 mM NaCl, 2.5 mM KCl, 1.2 mM NaH_2PO_4, 30 mM $NaHCO_3$, 20 mM Hepes, 25 mM glucose, 4 mM sodium ascorbate, 2 mM thiourea, 3 mM sodium pyruvate, 2 mM $MgSO_4(H_2O)_7$, 2 mM $CaCl_2(H_2O_2)$, and 2 M NaOH added until pH reached 7.3 to 7.4 and osmolarity was 300 to 310 mosmol. Patch pipettes were pulled from 1.5-mm borosilicate glass capillaries (World Precision Instruments; 4- to 8-MW resistance). Pipettes were filled with K-gluconate intracellular solution for intrinsic experiments. K-gluconate composition was 120 mM K-gluconate, 6 mM KCl, 10 mM Hepes, 4 mM adenosine 5′-triphosphate–Mg, 0.3 mM guanosine 5′-triphosphate–Na, and 0.1 mM EGTA and titrated to a pH of ~7.2 with KOH. During recordings, slices were transferred to a perfusion chamber and continuously perfused with artificial cerebrospinal fluid at 31 C at a rate of 4 to 7 ml/min: 119 mM NaCl, 2.5 mM KCl, 1 mM NaH_2PO_4, 26 mM $NaHCO_3$, 11 mM dextrose, 1.3 mM $MgSO_4(H_2O)_7$, and mM 2.5 $CaCl_2(H_2O_2)$. All recordings were performed in the NAc core in mCherry-positive cells that were visualized using CellSens software (Olympus). Cells were voltage clamped at −70 mV, and 15 current steps were injected starting at −100 pA and increasing in increments of 25 pA per step. For all patch-clamp experiments, cells collected from the same animal were grouped together for analysis. Elicited action potentials were recorded in current-clamp mode, counted, and analyzed using pClamp11 (Clampfit, Axon Instruments). Series access was monitored throughout recordings to ensure cells were only used if the access had not changed more than 10%. All drugs and reagents were obtained from Sigma-Aldrich.

Single-nuclei dissociation

Two weeks following surgery, animals [four *lacZ* and four *Reln* (two males and two females) per group] were briefly stunned before rapid decapitation. Brains were acutely blocked and NAc punches obtained, flash frozen, and stored at −80°C before nuclei isolation. Nuclei dissociation for snRNA-seq was performed as previously described (*20*). One GEM (gel beads in emulsion) well was used per sample to generate barcoded nuclei (10x Genomics, PN-1000123, PN-1000122).

Single-nucleus RNA sequencing

Acute and repeated cocaine

Genes not expressed in at least 10 cells were removed before analysis on the integrated R object containing both acute and repeated cocaine and saline samples generated for Phillips *et al.* (*38*). Subclustering was performed by first subsetting all D1-MSNs from the integrated acute and repeated Seurat object (*38*). Dimensionality reduction was performed on this subset of cells [DefaultAssay() = "Integrated"] via principal components analysis (PCA) retaining 17 principal components (PCs), followed by uniform manifold approximation and projection (UMAP) with 17 PCs as input. Cells were then clustered under a graph-based approach by first identifying *K*-nearest neighbors in PCA space and then clustering under a Louvain algorithm with a resolution of 0.1. Gini coefficients were calculated using the gini() function that is available in the reldist v1.6-6 package (*131*, *132*) using RNA expression values obtained with the Seurat function AverageExpression(). Differential gene expression testing was performed using DESeq2 v.1.40.2 (*126*) with a likelihood ratio test (LRT) to identify distinct genes among the D1-MSN clusters. Gini coefficient graphs were generated after merging the Gini coefficient matrix with the DESeq2 matrix for each cluster. Pearson correlations were calculated using the rmcorr v0.6.0 package with subject equal to the number of samples ($n = 8$) in the integrated dataset (*133*).

Reln CRISPRi

Libraries were constructed according to manufacturer's instructions using the Chromium Single Cell 3′ Library Construction Kit (10x Genomics, PN-1000190), which uses version 3 chemistry for gene expression. Nuclei (6221) from adult rat NAc were sequenced on the Illumina NovaSeq6000 at the University of Alabama at Birmingham Heflin Genomics Core to a depth of ~300,000 reads per nuclei. All raw fastq files were aligned to the Ensembl mRatBn7.2 (Rn7) genome using CellRanger v7.1.0 (*134*) with the associated Ensembl gene transfer format (gtf) file (version 105). CellRanger filtered outputs were analyzed with Seurat v4.3.0.1 (*135*) using R v4.3.1 (*136*) in RStudio v2023.06.1+524 as follows. First, to filter out background contamination, cell-free ambient RNA was removed using SoupX v.1.6.2 as previously described (*38*). Next, we continued quality filtering in R with Seurat v.4.3.0.1 (*135*) by removing nuclei containing <200 genes and >5% of reads mapping to the mitochondrial genome (5846 nuclei post-processing). The counts data for each individual were then normalized, scaled by a factor of 10,000, and log transformed. For each sample, we used Seurat to determine the 3000 genes with highest cell-to-cell variability; these sets of genes were used to identify "anchor" pairs of cells between samples with a shared pattern of gene expression (*137*). We then integrated the eight individual datasets based on the identified anchors, using the first 17 PCs. Downstream analysis was performed on the integrated dataset.

Expression for each gene in the integrated dataset was scaled to a mean of 0 and variance of 1 across cells. We used Seurat for initial dimensionality reduction and clustering as detailed below. We first performed dimensionality reduction via PCA retaining 17 PCs, followed by UMAP with the 17 previously identified PCs as input. Cells were then clustered under a graph-based approach by first identifying *K*-nearest neighbors in PCA space and then clustering under a Louvain algorithm with a resolution of 0.3. After initial clustering but before differential gene expression analysis, we used DoubletFinder v.2.0.3 (*138*) to identify and remove heterotypic doublets, a consequence of two cells of different types being captured in a single droplet and, thus, presenting as a single heterotypic "cell." We assumed a doublet formation rate of 4% based on 8000 cells loaded per GEM well, as indicated in the 10x Genomics library preparation documentation. After removing doublets, we repeated the dimensionality reduction and clustering steps detailed above. We matched the resulting clusters to specific cell types based on known marker genes from previous work (*38*).

To identify genes differentially expressed between *Reln* knockdown and *lacZ* controls, we conducted a differential expression analysis on a pseudobulked gene expression matrix created by summing counts for each gene within a sample (or single GEM well) and across cells within each cell type. Genes with mean counts <5 were removed. Differential expression analysis was conducted with DESeq2 v.1.40.2 (*126*) using a LRT with treatment condition as the main effect and controlling for the effect of sex to ensure that identified significant differential expression could be attributed to the treatment and not confounded by differences in response between sexes. To assess differential expression among cell types, we conducted a separate LRT with cell type as the main effect and controlling for sex. All R code for our snRNA-seq analyses is available at https://doi.org/10.5281/zenodo.14201265.

To correlate cell types between this study and prior work (*38*), the function FindMarkers() in the Seurat package was used to define marker genes using the default Wilcoxon rank sum test for both datasets. Marker gene sets were filtered for genes with an adjusted P value < 0.05. Marker gene lists and the relative enrichment [$\log_2$(fold-change)] relative to all other clusters for each cell type were then concatenated, with annotation as to which dataset each cell type originated from. Pearson's correlation was then calculated using the cor() function in R.

Gene ontology analysis was performed using the online tool, g:Profiler (*139*), using DEGs defined by DESeq2 with an adjusted P value < 0.05 in the D1-MSN cluster (28 genes; table S1). A custom gene set was used as background reference, consisting of all genes detected in the D1-MSN cluster (21,042 genes), with the "custom over all" option selected and Bonferroni was used for statistical correction.

Pseudotime calculations were performed using Monocle v3_1.3.5 (*140*) and Seurat v4.3.0 (*135*). A Seurat object containing D1-MSNs from male and female adult Sprague-Dawley rats from *lacZ* control and *Reln* knockdown groups (two males and two females per group) was subject to the standard dimensionality reduction and clustering workflow using 17 PCs and a resolution value of 0.1. *Reln* expression was removed from the RNA matrix before subclustering. Annotation, counts metadata, and cell barcode information were extracted from the Seurat object and reconstructed into a Monocle v3 cds object using new_cell_data_set(). Rather than reclustering, the UMAP coordinates were extracted from the Seurat object and added to the Monocle object. The trajectory graph was created using learn_graph(), and the root cell was chosen in the "inactivated" population that expressed *Drd1* and *Htr4* (*38*). Pseudotime values for each cell were exported from the cds object and added back to the Seurat object metadata.

Statistical analysis

Sample sizes were determined using a freely available calculator (www.stat.ubc.ca/~rollin/stats/ssize/n2.html). Transcriptional differences from RT-qPCR experiments were compared with an unpaired *t* test with Welch's correction, one-way analysis of variance (ANOVA) with Tukey's post hoc tests, or two-way ANOVA with Šidák's post hoc tests, where appropriate. CPP data were compared with a two-way ANOVA with Tukey's multiple comparisons test. smRNA-FISH expression differences were compared with nested *t* test analysis with correction for multiple comparisons where appropriate. Statistical significance was designated at $\alpha = 0.05$ for all analyses. Statistical and graphical analyses were performed with Prism software (GraphPad, La Jolla, CA). Statistical assumptions (e.g., normality and homogeneity for parametric tests) were formally tested and examined via boxplots. Full details on all statistical tests can be found in table S3.

Supplementary Materials

The PDF file includes:
Figs. S1 to S11
Legends for tables S1 to S3

Other Supplementary Material for this manuscript includes the following:
Tables S1 to S3

REFERENCES AND NOTES

1. R. A. Wise, Dopamine, learning and motivation. *Nat. Rev. Neurosci.* **5**, 483–494 (2004).
2. J. J. Day, M. F. Roitman, R. M. Wightman, R. M. Carelli, Associative learning mediates dynamic shifts in dopamine signaling in the nucleus accumbens. *Nat. Neurosci.* **10**, 1020–1028 (2007).
3. V. Pascoli, J. Terrier, A. Hiver, C. Lüscher, Sufficiency of mesolimbic dopamine neuron stimulation for the progression to addiction. *Neuron* **88**, 1054–1066 (2015).
4. M. G. Kutlu, J. E. Zachry, P. R. Melugin, S. A. Cajigas, M. F. Chevee, S. J. Kelly, B. Kutlu, L. Tian, C. A. Siciliano, E. S. Calipari, Dopamine release in the nucleus accumbens core signals perceived saliency. *Curr. Biol.* **31**, 4748–4761.e8 (2021).
5. G. F. Koob, N. D. Volkow, Neurobiology of addiction: A neurocircuitry analysis. *Lancet Psychiatry* **3**, 760–773 (2016).
6. G. Di Chiara, A. Imperato, Drugs abused by humans preferentially increase synaptic dopamine concentrations in the mesolimbic system of freely moving rats. *Proc. Natl. Acad. Sci. U.S.A.* **85**, 5274–5278 (1988).
7. J. F. Cheer, K. M. Wassum, L. A. Sombers, M. L. A. V. Heien, J. L. Ariansen, B. J. Aragona, P. E. M. Phillips, R. M. Wightman, Phasic dopamine release evoked by abused substances requires cannabinoid receptor activation. *J. Neurosci.* **27**, 791–795 (2007).
8. A. K. Lahiri, M. D. Bevan, Dopaminergic transmission rapidly and persistently enhances excitability of D1 receptor-expressing striatal projection neurons. *Neuron* **106**, 277–290. e6 (2020).
9. R. van Zessen, Y. Li, L. Marion-Poll, N. Hulo, J. Flakowski, C. Lüscher, Dynamic dichotomy of accumbal population activity underlies cocaine sensitization. *eLife* **10**, e66048 (2021).
10. B. Tan, C. J. Browne, T. Nöbauer, A. Vaziri, J. M. Friedman, E. J. Nestler, Drugs of abuse hijack a mesolimbic pathway that processes homeostatic need. *Science* **384**, eadk6742 (2024).
11. R. M. Carelli, J. Wondolowski, Selective encoding of cocaine versus natural rewards by nucleus accumbens neurons is not related to chronic drug exposure. *J. Neurosci.* **23**, 11214–11223 (2003).
12. B. Hope, B. Kosofsky, S. E. Hyman, E. J. Nestler, Regulation of immediate early gene expression and AP-1 binding in the rat nucleus accumbens by chronic cocaine. *Proc. Natl. Acad. Sci. U.S.A.* **89**, 5764–5768 (1992).
13. W. A. Carlezon, J. Thome, V. G. Olson, S. B. Lane-Ladd, E. S. Brodkin, N. Hiroi, R. S. Duman, R. L. Neve, E. J. Nestler, Regulation of cocaine reward by CREB. *Science* **282**, 2272–2275 (1998).

14. A. M. Graybiel, R. Moratalla, H. A. Robertson, Amphetamine and cocaine induce drug-specific activation of the c-fos gene in striosome-matrix compartments and limbic subdivisions of the striatum. *Proc. Natl. Acad. Sci. U.S.A.* **87**, 6912–6916 (1990).
15. M. D. Carpenter, Q. Hu, A. M. Bond, S. I. Lombroso, K. S. Czarnecki, C. J. Lim, H. Song, M. E. Wimmer, R. C. Pierce, E. A. Heller, Nr4a1 suppresses cocaine-induced behavior via epigenetic regulation of homeostatic target genes. *Nat. Commun.* **11**, 504 (2020).
16. S.-J. Xu, S. I. Lombroso, D. K. Fischer, M. D. Carpenter, D. M. Marchione, P. J. Hamilton, C. J. Lim, R. L. Neve, B. A. Garcia, M. E. Wimmer, R. C. Pierce, E. A. Heller, Chromatin-mediated alternative splicing regulates cocaine-reward behavior. *Neuron* **109**, 2943–2966.e8 (2021).
17. P. Mews, A. M. Cunningham, J. Scarpa, A. Ramakrishnan, E. M. Hicks, S. Bolnick, S. Garamszegi, L. Shen, D. C. Mash, E. J. Nestler, Convergent abnormalities in striatal gene networks in human cocaine use disorder and mouse cocaine administration models. *Sci. Adv.* **9**, eadd8946 (2023).
18. A.-C. Bobadilla, E. Dereschewitz, L. Vaccaro, J. A. Heinsbroek, M. D. Scofield, P. W. Kalivas, Cocaine and sucrose rewards recruit different seeking ensembles in the nucleus accumbens core. *Mol. Psychiatry* **25**, 3150–3163 (2020).
19. Y. Zhou, H. Zhu, Z. Liu, X. Chen, X. Su, C. Ma, Z. Tian, B. Huang, E. Yan, X. Liu, L. Ma, A ventral CA1 to nucleus accumbens core engram circuit mediates conditioned place preference for cocaine. *Nat. Neurosci.* **22**, 1986–1999 (2019).
20. K. E. Savell, J. J. Tuscher, M. E. Zipperly, C. G. Duke, R. A. Phillips, A. J. Bauman, S. Thukral, F. A. Sultan, N. A. Goska, L. Ianov, J. J. Day, A dopamine-induced gene expression signature regulates neuronal function and cocaine response. *Sci. Adv.* **6**, eaba4221 (2020).
21. E. Koya, S. A. Golden, B. K. Harvey, D. H. Guez-Barber, A. Berkow, D. E. Simmons, J. M. Bossert, S. G. Nair, J. L. Uejima, M. T. Marin, T. B. Mitchell, D. Farquhar, S. C. Ghosh, B. J. Mattson, B. T. Hope, Targeted disruption of cocaine-activated nucleus accumbens neurons prevents context-specific sensitization. *Nat. Neurosci.* **12**, 1069–1073 (2009).
22. V. Pascoli, M. Turiault, C. Lüscher, Reversal of cocaine-evoked synaptic potentiation resets drug-induced adaptive behaviour. *Nature* **481**, 71–75 (2011).
23. R. Chandra, J. D. Lenz, A. M. Gancarz, D. Chaudhury, G. L. Schroeder, M.-H. Han, J. F. Cheer, D. M. Dietz, M. K. Lobo, Optogenetic inhibition of D1R containing nucleus accumbens neurons alters cocaine-mediated regulation of Tiam1. *Front. Mol. Neurosci.* **6**, 13 (2013).
24. D. Lee, M. Creed, K. Jung, T. Stefanelli, D. J. Wendler, W. C. Oh, N. L. Mignocchi, C. Lüscher, H.-B. Kwon, Temporally precise labeling and control of neuromodulatory circuits in the mammalian brain. *Nat. Methods* **14**, 495–503 (2017).
25. B. W. Sortman, S. Rakela, S. Paprotna, B. Cerci, B. L. Warren, Nucleus accumbens neuronal ensembles vary with cocaine reinforcement in male and female rats. *Addict. Biol.* **29**, e13397 (2024).
26. E. S. Calipari, R. C. Bagot, I. Purushothaman, T. J. Davidson, J. T. Yorgason, C. J. Peña, D. M. Walker, S. T. Pirpinias, K. G. Guise, C. Ramakrishnan, K. Deisseroth, E. J. Nestler, In vivo imaging identifies temporal signature of D1 and D2 medium spiny neurons in cocaine reward. *Proc. Natl. Acad. Sci. U.S.A.* **113**, 2726–2731 (2016).
27. F. J. Nasif, K. Sidiropoulou, X.-T. Hu, F. J. White, Repeated cocaine administration increases membrane excitability of pyramidal neurons in the rat medial prefrontal cortex. *J. Pharmacol. Exp. Ther.* **312**, 1305–1313 (2005).
28. P. Mu, J. T. Moyer, M. Ishikawa, Y. Zhang, J. Panksepp, B. A. Sorg, O. M. Schlüter, Y. Dong, Exposure to cocaine dynamically regulates the intrinsic membrane excitability of nucleus accumbens neurons. *J. Neurosci.* **30**, 3689–3699 (2010).
29. E. J. Nestler, M. Barrot, D. W. Self, DeltaFosB: A sustained molecular switch for addiction. *Proc. Natl. Acad. Sci. U.S.A.* **98**, 11042–11046 (2001).
30. J. Zhang, L. Zhang, H. Jiao, Q. Zhang, D. Zhang, D. Lou, J. L. Katz, M. Xu, c-Fos facilitates the acquisition and extinction of cocaine-induced persistent changes. *J. Neurosci.* **26**, 13287–13296 (2006).
31. E. J. Nestler, C. Lüscher, The molecular basis of drug addiction: Linking epigenetic to synaptic and circuit mechanisms. *Neuron* **102**, 48–59 (2019).
32. E. Koya, F. C. Cruz, R. Ator, S. A. Golden, A. F. Hoffman, C. R. Lupica, B. T. Hope, Silent synapses in selectively activated nucleus accumbens neurons following cocaine sensitization. *Nat. Neurosci.* **15**, 1556–1562 (2012).
33. Y.-Y. Ma, B. R. Lee, X. Wang, C. Guo, L. Liu, R. Cui, Y. Lan, J. J. Balcita-Pedicino, M. E. Wolf, S. R. Sesack, Y. Shaham, O. M. Schlüter, Y. H. Huang, Y. Dong, Bidirectional modulation of incubation of cocaine craving by silent synapse-based remodeling of prefrontal cortex to accumbens projections. *Neuron* **83**, 1453–1467 (2014).
34. W. J. Wright, N. M. Graziane, P. A. Neumann, P. J. Hamilton, H. M. Cates, L. Fuerst, A. Spenceley, N. MacKinnon-Booth, K. Iyer, Y. H. Huang, Y. Shaham, O. M. Schlüter, E. J. Nestler, Y. Dong, Silent synapses dictate cocaine memory destabilization and reconsolidation. *Nat. Neurosci.* **23**, 32–46 (2020).
35. M. K. Lobo, H. E. Covington, D. Chaudhury, A. K. Friedman, H. Sun, D. Damez-Werno, D. M. Dietz, S. Zaman, J. W. Koo, P. J. Kennedy, E. Mouzon, M. Mogri, R. L. Neve, K. Deisseroth, M.-H. Han, E. J. Nestler, Cell type-specific loss of BDNF signaling mimics optogenetic control of cocaine reward. *Science* **330**, 385–390 (2010).
36. S. Z. Jiang, S. Sweat, S. P. Dahlke, K. Loane, G. Drossel, W. Xu, H. A. Tejeda, C. R. Gerfen, L. E. Eiden, Cocaine-dependent acquisition of locomotor sensitization and conditioned place preference requires D1 dopaminergic signaling through a cyclic AMP, NCS-Rapgef2, ERK, and Egr-1/Zif268 pathway. *J. Neurosci.* **41**, 711–725 (2021).
37. R. Chandra, M. Engeln, T. C. Francis, P. Konkalmatt, D. Patel, M. K. Lobo, A Role for peroxisome proliferator-activated receptor gamma coactivator-1α in nucleus accumbens neuron subtypes in cocaine action. *Biol. Psychiatry* **81**, 564–572 (2017).
38. R. A. Phillips, J. J. Tuscher, N. D. Fitzgerald, E. Wan, M. E. Zipperly, C. G. Duke, L. Ianov, J. J. Day, Distinct subpopulations of D1 medium spiny neurons exhibit unique transcriptional responsiveness to cocaine. *Mol. Cell. Neurosci.* **125**, 103849 (2023).
39. D. Guez-Barber, S. Fanous, S. A. Golden, R. Schrama, E. Koya, A. L. Stern, J. M. Bossert, B. K. Harvey, M. R. Picciotto, B. T. Hope, FACS identifies unique cocaine-induced gene regulation in selectively activated adult striatal neurons. *J. Neurosci.* **31**, 4251–4259 (2011).
40. S. A. Josselyn, S. Köhler, P. W. Frankland, Finding the engram. *Nat. Rev. Neurosci.* **16**, 521–534 (2015).
41. J.-H. Han, S. A. Kushner, A. P. Yiu, C. J. Cole, A. Matynia, R. A. Brown, R. L. Neve, J. F. Guzowski, A. J. Silva, S. A. Josselyn, Neuronal competition and selection during memory formation. *Science* **316**, 457–460 (2007).
42. H.-L. L. Hsiang, J. R. Epp, M. C. van den Oever, C. Yan, A. J. Rashid, N. Insel, L. Ye, Y. Niibori, K. Deisseroth, P. W. Frankland, S. A. Josselyn, Manipulating a "cocaine engram" in mice. *J. Neurosci.* **34**, 14115–14127 (2014).
43. J. Herz, Y. Chen, Reelin, lipoprotein receptors and synaptic plasticity. *Nat. Rev. Neurosci.* **7**, 850–859 (2006).
44. M. Trommsdorff, M. Gotthardt, T. Hiesberger, J. Shelton, W. Stockinger, J. Nimpf, R. E. Hammer, J. A. Richardson, J. Herz, Reeler/disabled-like disruption of neuronal migration in knockout mice lacking the VLDL receptor and ApoE receptor 2. *Cell* **97**, 689–701 (1999).
45. G. D'Arcangelo, G. G. Miao, S. C. Chen, H. D. Soares, J. I. Morgan, T. Curran, A protein related to extracellular matrix proteins deleted in the mouse mutant reeler. *Nature* **374**, 719–723 (1995).
46. F. Telese, Q. Ma, P. M. Perez, D. Notani, S. Oh, W. Li, D. Comoletti, K. A. Ohgi, H. Taylor, M. G. Rosenfeld, LRP8-Reelin-regulated neuronal enhancer signature underlying learning and memory formation. *Neuron* **86**, 696–710 (2015).
47. G. Di Chiara, Nucleus accumbens shell and core dopamine: Differential role in behavior and addiction. *Behav. Brain Res.* **137**, 75–114 (2002).
48. P. Voorn, L. J. M. J. Vanderschuren, H. J. Groenewegen, T. W. Robbins, C. M. A. Pennartz, Putting a spin on the dorsal-ventral divide of the striatum. *Trends Neurosci.* **27**, 468–474 (2004).
49. E. S. Lein, M. J. Hawrylycz, N. Ao, M. Ayres, A. Bensinger, A. Bernard, A. F. Boe, M. S. Boguski, K. S. Brockway, E. J. Byrnes, L. Chen, L. Chen, T.-M. Chen, M. C. Chin, J. Chong, B. E. Crook, A. Czaplinska, C. N. Dang, S. Datta, N. R. Dee, A. L. Desaki, T. Desta, E. Diep, T. A. Dolbeare, M. J. Donelan, H.-W. Dong, J. G. Dougherty, B. J. Duncan, A. J. Ebbert, G. Eichele, L. K. Estin, C. Faber, B. A. Facer, R. Fields, S. R. Fischer, T. P. Fliss, C. Frensley, S. N. Gates, K. J. Glattfelder, K. R. Halverson, M. R. Hart, J. G. Hohmann, M. P. Howell, D. P. Jeung, R. A. Johnson, P. T. Karr, R. Kawal, J. M. Kidney, R. H. Knapik, C. L. Kuan, J. H. Lake, A. R. Laramee, K. D. Larsen, C. Lau, T. A. Lemon, A. J. Liang, Y. Liu, L. T. Luong, J. Michaels, J. J. Morgan, R. J. Morgan, M. T. Mortrud, N. F. Mosqueda, L. L. Ng, R. Ng, G. J. Orta, C. C. Overly, T. H. Pak, S. E. Parry, S. D. Pathak, O. C. Pearson, R. B. Puchalski, Z. L. Riley, H. R. Rockett, S. A. Rowland, J. J. Royall, M. J. Ruiz, N. R. Sarno, K. Schaffnit, N. V. Shapovalova, T. Sivisay, C. R. Slaughterbeck, S. C. Smith, K. A. Smith, B. I. Smith, A. J. Sodt, N. N. Stewart, K.-R. Stumpf, S. M. Sunkin, M. Sutram, A. Tam, C. D. Teemer, C. Thaller, C. L. Thompson, L. R. Varnam, A. Visel, R. M. Whitlock, P. E. Wohnoutka, C. K. Wolkey, V. Y. Wong, M. Wood, M. B. Yaylaoglu, R. C. Young, B. L. Youngstrom, X. F. Yuan, B. Zhang, T. A. Zwingman, A. R. Jones, Genome-wide atlas of gene expression in the adult mouse brain. *Nature* **445**, 168–176 (2007).
50. M. J. Hawrylycz, E. S. Lein, A. L. Guillozet-Bongaarts, E. H. Shen, L. Ng, J. A. Miller, L. N. van de Lagemaat, K. A. Smith, A. Ebbert, Z. L. Riley, C. Abajian, C. F. Beckmann, A. Bernard, D. Bertagnolli, A. F. Boe, P. M. Cartagena, M. M. Chakravarty, M. Chapin, J. Chong, R. A. Dalley, B. D. Daly, C. Dang, S. Datta, N. Dee, T. A. Dolbeare, V. Faber, D. Feng, D. R. Fowler, J. Goldy, B. W. Gregor, Z. Haradon, D. R. Haynor, J. G. Hohmann, S. Horvath, R. E. Howard, A. Jeromin, J. M. Jochim, M. Kinnunen, C. Lau, E. T. Lazarz, C. Lee, T. A. Lemon, L. Li, Y. Li, J. A. Morris, C. C. Overly, P. D. Parker, S. E. Parry, M. Reding, J. J. Royall, J. Schulkin, P. A. Sequeira, C. R. Slaughterbeck, S. C. Smith, A. J. Sodt, S. M. Sunkin, B. E. Swanson, M. P. Vawter, D. Williams, P. Wohnoutka, H. R. Zielke, D. H. Geschwind, P. R. Hof, S. M. Smith, C. Koch, S. G. N. Grant, A. R. Jones, An anatomically comprehensive atlas of the adult human brain transcriptome. *Nature* **489**, 391–399 (2012).
51. M. N. Tran, K. R. Maynard, A. Spangler, L. A. Huuki, K. D. Montgomery, V. Sadashivaiah, M. Tippani, B. K. Barry, D. B. Hancock, S. C. Hicks, J. E. Kleinman, T. M. Hyde, L. Collado-Torres, A. E. Jaffe, K. Martinowich, Single-nucleus transcriptome analysis reveals cell-type-specific molecular signatures across reward circuitry in the human brain. *Neuron* **109**, 3088–3103.e5 (2021).

52. G. de Guglielmo, A. Iemolo, A. Nur, A. Turner, P. Montilla-Perez, A. Martinez, C. Crook, A. Roberts, F. Telese, Reelin deficiency exacerbates cocaine-induced hyperlocomotion by enhancing neuronal activity in the dorsomedial striatum. *Genes Brain Behav.* **21**, e12828 (2022).
53. D. S. Falconer, Two new mutants, 'trembler' and 'reeler', with neurological actions in the house mouse (*Mus musculus* L.). *J. Genet.* **50**, 192–205 (1951).
54. A. Sobue, I. Kushima, T. Nagai, W. Shan, T. Kohno, B. Aleksic, Y. Aoyama, D. Mori, Y. Arioka, N. Kawano, M. Yamamoto, M. Hattori, T. Nabeshima, K. Yamada, N. Ozaki, Genetic and animal model analyses reveal the pathogenic role of a novel deletion of RELN in schizophrenia. *Sci. Rep.* **8**, 13046 (2018).
55. V. de Bergeyck, K. Nakajima, C. Lambert de Rouvroit, B. Naerhuyzen, A. M. Goffinet, T. Miyata, M. Ogawa, K. Mikoshiba, A truncated Reelin protein is produced but not secreted in the 'Orleans' reeler mutation (*Reln*$^{rl\text{-}Orl}$). *Brain Res. Mol. Brain Res.* **50**, 85–90 (1997).
56. T. Takahara, T. Ohsumi, J. Kuromitsu, K. Shibata, N. Sasaki, Y. Okazaki, H. Shibata, S. Sato, A. Yoshiki, M. Kusakabe, M. Muramatsu, M. Ueki, K. Okuda, Y. Hayashizaki, Dysfunction of the Orleans reeler gene arising from exon skipping due to transposition of a full-length copy of an active L1 sequence into the skipped exon. *Hum. Mol. Genet.* **5**, 989–993 (1996).
57. C. R. Wasser, J. Herz, Reelin: Neurodevelopmental architect and homeostatic regulator of excitatory synapses. *J. Biol. Chem.* **292**, 1330–1338 (2017).
58. K. E. Savell, S. V. Bach, M. E. Zipperly, J. S. Revanna, N. A. Goska, J. J. Tuscher, C. G. Duke, F. A. Sultan, J. N. Burke, D. Williams, L. Ianov, J. J. Day, A neuron-optimized CRISPR/dCas9 activation system for robust and specific gene regulation. *eNeuro* **6**, ENEURO.0495–18.2019 (2019).
59. C. G. Duke, S. V. Bach, J. S. Revanna, F. A. Sultan, N. T. Southern, M. N. Davis, N. V. N. Carullo, A. J. Bauman, R. A. Phillips, J. J. Day, An improved crispr/dcas9 interference tool for neuronal gene suppression. *Front. Genome Ed.* **2**, 9 (2020).
60. N. C. Yeo, A. Chavez, A. Lance-Byrne, Y. Chan, D. Menn, D. Milanova, C.-C. Kuo, X. Guo, S. Sharma, A. Tung, R. J. Cecchi, M. Tuttle, S. Pradhan, E. T. Lim, N. Davidsohn, M. R. Ebrahimkhani, J. J. Collins, N. E. Lewis, S. Kiani, G. M. Church, An enhanced CRISPR repressor for targeted mammalian gene regulation. *Nat. Methods* **15**, 611–616 (2018).
61. J. W. Squair, M. Gautier, C. Kathe, M. A. Anderson, N. D. James, T. H. Hutson, R. Hudelle, T. Qaiser, K. J. E. Matson, Q. Barraud, A. J. Levine, G. La Manno, M. A. Skinnider, G. Courtine, Confronting false discoveries in single-cell differential expression. *Nat. Commun.* **12**, 5692 (2021).
62. E. Valjent, J. Bertran-Gonzalez, B. Aubier, P. Greengard, D. Hervé, J.-A. Girault, Mechanisms of locomotor sensitization to drugs of abuse in a two-injection protocol. *Neuropsychopharmacology* **35**, 401–415 (2010).
63. T. E. Robinson, K. C. Berridge, The neural basis of drug craving: An incentive-sensitization theory of addiction. *Brain Res. Brain Res. Rev.* **18**, 247–291 (1993).
64. K. Sakai, H. Shoji, T. Kohno, T. Miyakawa, M. Hattori, Mice that lack the C-terminal region of Reelin exhibit behavioral abnormalities related to neuropsychiatric disorders. *Sci. Rep.* **6**, 28636 (2016).
65. A. Iemolo, P. Montilla-Perez, J. Nguyen, V. B. Risbrough, M. A. Taffe, F. Telese, Reelin deficiency contributes to long-term behavioral abnormalities induced by chronic adolescent exposure to Δ9-tetrahydrocannabinol in mice. *Neuropharmacology* **187**, 108495 (2021).
66. B. J. Mattson, E. Koya, D. E. Simmons, T. B. Mitchell, A. Berkow, H. S. Crombag, B. T. Hope, Context-specific sensitization of cocaine-induced locomotor activity and associated neuronal ensembles in rat nucleus accumbens. *Eur. J. Neurosci.* **27**, 202–212 (2008).
67. D. M. Walker, H. M. Cates, Y.-H. E. Loh, I. Purushothaman, A. Ramakrishnan, K. M. Cahill, C. K. Lardner, A. Godino, H. G. Kronman, J. Rabkin, Z. S. Lorsch, P. Mews, M. A. Doyle, J. Feng, B. Labonté, J. W. Koo, R. C. Bagot, R. W. Logan, M. L. Seney, E. S. Calipari, E. J. Nestler, Cocaine self-administration alters transcriptome-wide responses in the brain's reward circuitry. *Biol. Psychiatry* **84**, 867–880 (2018).
68. R. R. Campbell, S. Chen, J. H. Beardwood, A. J. López, L. V. Pham, A. M. Keiser, J. E. Childs, D. P. Matheos, V. Swarup, P. Baldi, M. A. Wood, Cocaine induces paradigm-specific changes to the transcriptome within the ventral tegmental area. *Neuropsychopharmacology* **46**, 1768–1779 (2021).
69. R. M. Carelli, Nucleus accumbens cell firing during goal-directed behaviors for cocaine vs. 'natural' reinforcement. *Physiol. Behav.* **76**, 379–387 (2002).
70. A. Stipanovich, E. Valjent, M. Matamales, A. Nishi, J.-H. Ahn, M. Maroteaux, J. Bertran-Gonzalez, K. Brami-Cherrier, H. Enslen, A.-G. Corbillé, O. Filhol, A. C. Nairn, P. Greengard, D. Hervé, J.-A. Girault, A phosphatase cascade by which rewarding stimuli control nucleosomal response. *Nature* **453**, 879–884 (2008).
71. R. A. Phillips, E. Wan, J. J. Tuscher, D. Reid, O. R. Drake, L. Ianov, J. J. Day, Temporally specific gene expression and chromatin remodeling programs regulate a conserved Pdyn enhancer. *eLife* **12**, RP89993 (2023).
72. C. D. Teague, E. J. Nestler, Key transcription factors mediating cocaine-induced plasticity in the nucleus accumbens. *Mol. Psychiatry* **27**, 687–709 (2022).
73. N. V. N. Carullo, R. A. Phillips Iii, R. C. Simon, S. A. R. Soto, J. E. Hinds, A. J. Salisbury, J. S. Revanna, K. D. Bunner, L. Ianov, F. A. Sultan, K. E. Savell, C. A. Gersbach, J. J. Day, Enhancer RNAs predict enhancer-gene regulatory links and are critical for enhancer function in neuronal systems. *Nucleic Acids Res.* **48**, 9550–9570 (2020).
74. M. E. Zipperly, F. A. Sultan, G.-E. Graham, A. C. Brane, N. A. Simpkins, N. V. N. Carullo, L. Ianov, J. J. Day, Regulation of dopamine-dependent transcription and cocaine action by Gadd45b. *Neuropsychopharmacology* **46**, 709–720 (2021).
75. O. Garritsen, E. Y. van Battum, L. M. Grossouw, R. J. Pasterkamp, Development, wiring and function of dopamine neuron subtypes. *Nat. Rev. Neurosci.* **24**, 134–152 (2023).
76. S. Nishikawa, S. Goto, K. Yamada, T. Hamasaki, Y. Ushio, Lack of Reelin causes malpositioning of nigral dopaminergic neurons: Evidence from comparison of normal and *Reln*^{rl} mutant mice. *J. Comp. Neurol.* **461**, 166–173 (2003).
77. U. Beffert, E. J. Weeber, A. Durudas, S. Qiu, I. Masiulis, J. D. Sweatt, W.-P. Li, G. Adelmann, M. Frotscher, R. E. Hammer, J. Herz, Modulation of synaptic plasticity and memory by Reelin involves differential splicing of the lipoprotein receptor Apoer2. *Neuron* **47**, 567–579 (2005).
78. S. Qiu, L. F. Zhao, K. M. Korwek, E. J. Weeber, Differential reelin-induced enhancement of NMDA and AMPA receptor activity in the adult hippocampus. *J. Neurosci.* **26**, 12943–12955 (2006).
79. C. M. Teixeira, E. D. Martín, I. Sahún, N. Masachs, L. Pujadas, A. Corvelo, C. Bosch, D. Rossi, A. Martinez, R. Maldonado, M. Dierssen, E. Soriano, Overexpression of Reelin prevents the manifestation of behavioral phenotypes related to schizophrenia and bipolar disorder. *Neuropsychopharmacology* **36**, 2395–2405 (2011).
80. M. Mahgoub, L. M. Monteggia, Epigenetics and psychiatry. *Neurotherapeutics* **10**, 734–741 (2013).
81. A. Guidotti, J. Auta, J. M. Davis, V. Di-Giorgi-Gerevini, Y. Dwivedi, D. R. Grayson, F. Impagnatiello, G. Pandey, C. Pesold, R. Sharma, D. Uzunov, E. Costa, Decrease in reelin and glutamic acid decarboxylase67 (GAD67) expression in schizophrenia and bipolar disorder: A postmortem brain study. *Arch. Gen. Psychiatry* **57**, 1061–1069 (2000).
82. I. Knuesel, Reelin-mediated signaling in neuropsychiatric and neurodegenerative diseases. *Prog. Neurobiol.* **91**, 257–274 (2010).
83. B. Escudero, M. Moya, L. López-Valencia, F. Arias, L. Orio, Reelin plasma levels identify cognitive decline in alcohol use disorder patients during early abstinence: The influence of APOE4 expression. *Int. J. Neuropsychopharmacol.* **26**, 545–556 (2023).
84. C. Lane-Donovan, G. T. Philips, C. R. Wasser, M. S. Durakoglugil, I. Masiulis, A. Upadhaya, T. Pohlkamp, C. Coskun, T. Kotti, L. Steller, R. E. Hammer, M. Frotscher, H. H. Bock, J. Herz, Reelin protects against amyloid β toxicity in vivo. *Sci. Signal.* **8**, ra67 (2015).
85. F. Lopera, C. Marino, A. S. Chandrahas, M. O'Hare, N. D. Villalba-Moreno, D. Aguillon, A. Baena, J. S. Sanchez, C. Vila-Castelar, L. R. Gomez, N. Chmielewska, G. M. Oliveira, J. L. Littau, K. Hartmann, K. Park, S. Krasemann, M. Glatzel, D. Schoemaker, L. Gonzalez-Buendia, S. Delgado-Tirado, S. Arevalo-Alquichire, K. L. Saez-Torres, D. Amarnani, L. A. Kim, R. C. Mazzarino, H. Gordon, Y. Bocanegra, A. Villegas, X. Gai, M. Bootwalla, J. Ji, L. Shen, K. S. Kosik, Y. Su, Y. Chen, A. Schultz, R. A. Sperling, K. Johnson, E. M. Reiman, D. Sepulveda-Falla, J. F. Arboleda-Velasquez, Y. T. Quiroz, Resilience to autosomal dominant Alzheimer's disease in a Reelin-COLBOS heterozygous man. *Nat. Med.* **29**, 1243–1252 (2023).
86. Y. Jossin, Reelin functions, mechanisms of action and signaling pathways during brain development and maturation. *Biomolecules* **10**, 964 (2020).
87. H. H. Bock, P. May, Canonical and Non-canonical Reelin Signaling. *Front. Cell. Neurosci.* **10**, 166 (2016).
88. R. Chen, T. R. Blosser, M. N. Djekidel, J. Hao, A. Bhattacherjee, W. Chen, L. M. Tuesta, X. Zhuang, Y. Zhang, Decoding molecular and cellular heterogeneity of mouse nucleus accumbens. *Nat. Neurosci.* **24**, 1757–1771 (2021).
89. M. Pardo, S. Gregorio, E. Montalban, L. Pujadas, A. Elias-Tersa, N. Masachs, A. Vílchez-Acosta, A. Parent, C. Auladell, J.-A. Girault, M. Vila, A. C. Nairn, Y. Manso, E. Soriano, Adult-specific Reelin expression alters striatal neuronal organization: Implications for neuropsychiatric disorders. *Front. Cell. Neurosci.* **17**, 1143319 (2023).
90. J. T. Rogers, I. Rusiana, J. Trotter, L. Zhao, E. Donaldson, D. T. S. Pak, L. W. Babus, M. Peters, J. L. Banko, P. Chavis, G. W. Rebeck, H.-S. Hoe, E. J. Weeber, Reelin supplementation enhances cognitive ability, synaptic plasticity, and dendritic spine density. *Learn. Mem.* **18**, 558–564 (2011).
91. M. S. Durakoglugil, C. R. Wasser, C. H. Wong, T. Pohlkamp, X. Xian, C. Lane-Donovan, K. Fritschle, L. Naestle, J. Herz, Reelin regulates neuronal excitability through striatal-enriched protein tyrosine phosphatase ($STEP_{61}$) and calcium permeable AMPARs in an NMDAR-dependent manner. *J. Neurosci.* **41**, 7340–7349 (2021).
92. J.-W. Kim, J. Herz, E. T. Kavalali, L. M. Monteggia, A key requirement for synaptic Reelin signaling in ketamine-mediated behavioral and synaptic action. *Proc. Natl. Acad. Sci. U.S.A.* **118**, e2103079118 (2021).
93. H. Abraham, G. Meyer, Reelin-expressing neurons in the postnatal and adult human hippocampal formation. *Hippocampus* **13**, 715–727 (2003).
94. A. Saunders, E. Z. Macosko, A. Wysoker, M. Goldman, F. M. Krienen, H. de Rivera, E. Bien, M. Baum, L. Bortolin, S. Wang, A. Goeva, J. Nemesh, N. Kamitaki, S. Brumbaugh, D. Kulp, S. A. McCarroll, Molecular diversity and specializations among the cells of the adult mouse brain. *Cell* **174**, 1015–1030.e16 (2018).

95. M. Sheng, M. E. Greenberg, The regulation and function of c-fos and other immediate early genes in the nervous system. *Neuron* **4**, 477–485 (1990).
96. M. R. Lyons, A. E. West, Mechanisms of specificity in neuronal activity-regulated gene transcription. *Prog. Neurobiol.* **94**, 259–295 (2011).
97. E.-L. Yap, M. E. Greenberg, Activity-regulated transcription: Bridging the gap between neural activity and behavior. *Neuron* **100**, 330–348 (2018).
98. L. G. Reijmers, B. L. Perkins, N. Matsuo, M. Mayford, Localization of a stable neural correlate of associative memory. *Science* **317**, 1230–1233 (2007).
99. C. J. Guenthner, K. Miyamichi, H. H. Yang, H. C. Heller, L. Luo, Permanent genetic access to transiently active neurons via TRAP: Targeted recombination in active populations. *Neuron* **78**, 773–784 (2013).
100. N. R. Wall, P. A. Neumann, K. T. Beier, A. K. Mokhtari, L. Luo, R. C. Malenka, Complementary genetic targeting and monosynaptic input mapping reveal recruitment and refinement of distributed corticostriatal ensembles by cocaine. *Neuron* **104**, 916–930.e5 (2019).
101. L. A. DeNardo, C. D. Liu, W. E. Allen, E. L. Adams, D. Friedmann, L. Fu, C. J. Guenthner, M. Tessier-Lavigne, L. Luo, Temporal evolution of cortical ensembles promoting remote memory retrieval. *Nat. Neurosci.* **22**, 460–469 (2019).
102. B. L. Bloodgood, N. Sharma, H. A. Browne, A. Z. Trepman, M. E. Greenberg, The activity-dependent transcription factor NPAS4 regulates domain-specific inhibition. *Nature* **503**, 121–125 (2013).
103. O. Roethler, E. Zohar, K. Cohen-Kashi Malina, L. Bitan, H. W. Gabel, I. Spiegel, Single genomic enhancers drive experience-dependent GABAergic plasticity to maintain sensory processing in the adult cortex. *Neuron* **111**, 2693–2708.e8 (2023).
104. E. L. Yap, N. L. Pettit, C. P. Davis, M. A. Nagy, D. A. Harmin, E. Golden, O. Dagliyan, C. Lin, S. Rudolph, N. Sharma, E. C. Griffith, C. D. Harvey, M. E. Greenberg, Bidirectional perisomatic inhibitory plasticity of a Fos neuronal network. *Nature* **590**, 115–121 (2021).
105. A. P. Yiu, V. Mercaldo, C. Yan, B. Richards, A. J. Rashid, H.-L. L. Hsiang, J. Pressey, V. Mahadevan, M. M. Tran, S. A. Kushner, M. A. Woodin, P. W. Frankland, S. A. Josselyn, Neurons are recruited to a memory trace based on relative neuronal excitability immediately before training. *Neuron* **83**, 722–735 (2014).
106. Y. Zhou, J. Won, M. G. Karlsson, M. Zhou, T. Rogerson, J. Balaji, R. Neve, P. Poirazi, A. J. Silva, CREB regulates excitability and the allocation of memory to subsets of neurons in the amygdala. *Nat. Neurosci.* **12**, 1438–1443 (2009).
107. A. J. Mocle, A. I. Ramsaran, A. D. Jacob, A. J. Rashid, A. Luchetti, L. M. Tran, B. A. Richards, P. W. Frankland, S. A. Josselyn, Excitability mediates allocation of pre-configured ensembles to a hippocampal engram supporting contextual conditioned threat in mice. *Neuron* **112**, 1487–1497.e6 (2024).
108. K. Bell, P. Duffy, P. W. Kalivas, Context-specific enhancement of glutamate transmission by cocaine. *Neuropsychopharmacology* **23**, 335–344 (2000).
109. G. Hotsenpiller, M. Giorgetti, M. E. Wolf, Alterations in behaviour and glutamate transmission following presentation of stimuli previously associated with cocaine exposure. *Eur. J. Neurosci.* **14**, 1843–1855 (2001).
110. E. Brai, S. Marathe, S. Astori, N. B. Fredj, E. Perry, C. Lamy, A. Scotti, L. Alberi, Notch1 regulates hippocampal plasticity through interaction with the reelin pathway, glutamatergic transmission and CREB signaling. *Front. Cell. Neurosci.* **9**, 447 (2015).
111. D. Avey, S. Sankararaman, A. K. Y. Yim, R. Barve, J. Milbrandt, R. D. Mitra, Single-cell RNA-seq uncovers a robust transcriptional response to morphine by glia. *Cell Rep.* **24**, 3619–3629.e4 (2018).
112. H. Matsuzaki, Y. Minabe, K. Nakamura, K. Suzuki, Y. Iwata, Y. Sekine, K. J. Tsuchiya, G. Sugihara, S. Suda, N. Takei, D. Nakahara, K. Hashimoto, A. C. Nairn, N. Mori, K. Sato, Disruption of reelin signaling attenuates methamphetamine-induced hyperlocomotion. *Eur. J. Neurosci.* **25**, 3376–3384 (2007).
113. M. van den Buuse, P. Halley, R. Hill, M. Labots, S. Martin, Altered N-methyl-D-aspartate receptor function in reelin heterozygous mice: Male-female differences and comparison with dopaminergic activity. *Prog. Neuropsychopharmacol. Biol. Psychiatry* **37**, 237–246 (2012).
114. T. Blasiak, W. Czubak, A. Ignaciak, M. H. Lewandowski, A new approach to detection of the bregma point on the rat skull. *J. Neurosci. Methods* **185**, 199–203 (2010).
115. R. A. Phillips III, J. J. Tuscher, S. L. Black, E. Andraka, N. D. Fitzgerald, L. Ianov, J. J. Day, An atlas of transcriptionally defined cell populations in the rat ventral tegmental area. *Cell Rep.* **39**, 110616 (2022).
116. E. Andraka, R. A. Phillips, K. L. Brida, J. J. Day, Chst9 marks a spatially and transcriptionally unique population of *Oprm1*-expressing neurons in the nucleus accumbens. *Addict. Neurosci.* **11**, 100153 (2024).
117. P. Bankhead, M. B. Loughrey, J. A. Fernández, Y. Dombrowski, D. G. McArt, P. D. Dunne, S. McQuaid, R. T. Gray, L. J. Murray, H. G. Coleman, J. A. James, M. Salto-Tellez, P. W. Hamilton, QuPath: Open source software for digital pathology image analysis. *Sci. Rep.* **7**, 16878 (2017).
118. B. K. Lipska, A. Deep-Soboslay, C. S. Weickert, T. M. Hyde, C. E. Martin, M. M. Herman, J. E. Kleinman, Critical factors in gene expression in postmortem human brain: Focus on studies in schizophrenia. *Biol. Psychiatry* **60**, 650–658 (2006).
119. K. R. Maynard, M. Tippani, Y. Takahashi, B. N. Phan, T. M. Hyde, A. E. Jaffe, K. Martinowich, dotdotdot: An automated approach to quantify multiplex single molecule fluorescent in situ hybridization (smFISH) images in complex tissues. *Nucleic Acids Res.* **48**, e66 (2020).
120. P. A. Ewels, A. Peltzer, S. Fillinger, H. Patel, J. Alneberg, A. Wilm, M. U. Garcia, P. Di Tommaso, S. Nahnsen, The nf-core framework for community-curated bioinformatics pipelines. *Nat. Biotechnol.* **38**, 276–278 (2020).
121. P. Di Tommaso, M. Chatzou, E. W. Floden, P. P. Barja, E. Palumbo, C. Notredame, Nextflow enables reproducible computational workflows. *Nat. Biotechnol.* **35**, 316–319 (2017).
122. A. Dobin, C. A. Davis, F. Schlesinger, J. Drenkow, C. Zaleski, S. Jha, P. Batut, M. Chaisson, T. R. Gingeras, STAR: Ultrafast universal RNA-seq aligner. *Bioinformatics* **29**, 15–21 (2013).
123. H. Li, B. Handsaker, A. Wysoker, T. Fennell, J. Ruan, N. Homer, G. Marth, G. Abecasis, R. Durbin, 1000 Genome Project Data Processing Subgroup, The Sequence Alignment/Map format and SAMtools. *Bioinformatics* **25**, 2078–2079 (2009).
124. Y. Liao, G. K. Smyth, W. Shi, The R package Rsubread is easier, faster, cheaper and better for alignment and quantification of RNA sequencing reads. *Nucleic Acids Res.* **47**, e47 (2019).
125. P. Ewels, M. Magnusson, S. Lundin, M. Käller, MultiQC: Summarize analysis results for multiple tools and samples in a single report. *Bioinformatics* **32**, 3047–3048 (2016).
126. M. I. Love, W. Huber, S. Anders, Moderated estimation of fold change and dispersion for RNA-seq data with DESeq2. *Genome Biol.* **15**, 550 (2014).
127. Y. Benjamini, Y. Hochberg, Controlling the false discovery rate: A practical and powerful approach to multiple testing. *J. R. Stat. Soc. Series B Methodol.* **57**, 289–300 (1995).
128. S. Bae, J. Park, J.-S. Kim, Cas-OFFinder: A fast and versatile algorithm that searches for potential off-target sites of Cas9 RNA-guided endonucleases. *Bioinformatics* **30**, 1473–1475 (2014).
129. M. Lawrence, W. Huber, H. Pagès, P. Aboyoun, M. Carlson, R. Gentleman, M. T. Morgan, V. J. Carey, Software for computing and annotating genomic ranges. *PLoS Comput. Biol.* **9**, e1003118 (2013).
130. E. T. Jorgensen, A. E. Gonzalez, J. H. Harkness, D. M. Hegarty, A. Thakar, D. J. Burchi, J. A. Aadland, S. A. Aicher, B. A. Sorg, T. E. Brown, Cocaine memory reactivation induces functional adaptations within parvalbumin interneurons in the rat medial prefrontal cortex. *Addict. Biol.* **26**, e12947 (2021).
131. C. Gini, Measurement of inequality of incomes. *Econ. J.* **31**, 124–126 (1921).
132. M. S. Handcock, M. Morris, *Relative Distribution Methods in the Social Sciences* (Springer-Verlag, 1999).
133. J. Z. Bakdash, L. R. Marusich, Repeated measures correlation. *Front. Psychol.* **8**, 456 (2017).
134. G. X. Y. Zheng, J. M. Terry, P. Belgrader, P. Ryvkin, Z. W. Bent, R. Wilson, S. B. Ziraldo, T. D. Wheeler, G. P. Mc Dermott, J. Zhu, M. T. Gregory, J. Shuga, L. Montesclaros, J. G. Underwood, D. A. Masquelier, S. Y. Nishimura, M. Schnall-Levin, P. W. Wyatt, C. M. Hindson, R. Bharadwaj, A. Wong, K. D. Ness, L. W. Beppu, H. J. Deeg, C. M. Farland, K. R. Loeb, W. J. Valente, N. G. Ericson, E. A. Stevens, J. P. Radich, T. S. Mikkelsen, B. J. Hindson, J. H. Bielas, Massively parallel digital transcriptional profiling of single cells. *Nat. Commun.* **8**, 14049 (2017).
135. Y. Hao, S. Hao, E. Andersen-Nissen, W. M. Mauck III, S. Zheng, A. Butler, M. J. Lee, A. J. Wilk, C. Darby, M. Zager, P. Hoffman, M. Stoeckius, E. Papalexi, E. P. Mimitou, J. Jain, A. Srivastava, T. Stuart, L. M. Fleming, B. Yeung, A. J. Rogers, J. M. M. Elrath, C. A. Blish, R. Gottardo, P. Smibert, R. Satija, Integrated analysis of multimodal single-cell data. *Cell* **184**, 3573–3587.e29 (2021).
136. R Core Team, R: A Language and Environment for Statistical Computing (R Foundation for Statistical Computing, 2023).
137. T. Stuart, A. Butler, P. Hoffman, C. Hafemeister, E. Papalexi, W. M. Mauck III, Y. Hao, M. Stoeckius, P. Smibert, R. Satija, Comprehensive integration of single-cell data. *Cell* **177**, 1888–1902.e21 (2019).
138. C. S. McGinnis, L. M. Murrow, Z. J. Gartner, DoubletFinder: Doublet detection in single-cell RNA sequencing data using artificial nearest neighbors. *Cell Syst.* **8**, 329–337.e4 (2019).
139. L. Kolberg, U. Raudvere, I. Kuzmin, P. Adler, J. Vilo, H. Peterson, g:Profiler-interoperable web service for functional enrichment analysis and gene identifier mapping (2023 update). *Nucleic Acids Res.* **51**, W207–W212 (2023).
140. J. Cao, M. Spielmann, X. Qiu, X. Huang, D. M. Ibrahim, A. J. Hill, F. Zhang, S. Mundlos, L. Christiansen, F. J. Steemers, C. Trapnell, J. Shendure, The single-cell transcriptional landscape of mammalian organogenesis. *Nature* **566**, 496–502 (2019).

Acknowledgments: We thank all current and former Day Lab members for assistance and support, as well as N. Davis, K. Savell, and N. Boyle for assistance. We acknowledge support from the University of Alabama at Birmingham Biological Data Science Core (RRID:SCR_021766), the UAB Heflin Center for Genomic Sciences, and the UAB Flow Cytometry and Single Cell Core Facility. **Funding:** This work was supported by NIH grants DP1DA039650 and R01DA053743 (J.J.D.), F30DA057821 (K.L.B.), and grant R01DA053581 (K.M.); McKnight Foundation Neurobiology of Brain Disorders Award (J.J.D.); Lieber Institute for Brain Development (K.M. and K.R.M.); Civitan International Research Center at UAB (L.I.); and Civitan International Research Center Emerging Scholars Award (K.L.B.). **Author**

contributions: Conceptualization: K.L.B., E.T.J., T.M.H., M.E.Z., and J.J.D. Methodology: K.L.B., E.T.J., E.K.M., J.J.T., M.E.Z., and T.M.H. Investigation: K.L.B., R.A.P., E.T.J., E.K.M., J.J.T., M.E.Z., K.D.M., T.M.H., K.R.M., and J.J.D. Formal analysis: K.L.B., R.A.P., E.T.J., C.E.N., M.T., M.E.Z., K.R.M., and J.J.D. Software: K.L.B., R.A.P., C.E.N., M.T., L.I., and J.J.D. Resources: K.L.B., E.T.J., K.M., T.M.H., K.R.M., and J.J.D. Funding acquisition: K.L.B., K.M., T.M.H., and J.J.D. Data curation: K.L.B., C.E.N., M.T., T.M.H., and J.J.D. Visualization: K.L.B., R.A.P., E.T.J., M.T., J.J.D., and C.E.N. Validation: K.L.B., R.A.P., E.K.M., M.E.Z., and J.J.D. Project administration: K.L.B, T.M.H., K.R.M., and J.J.D. Supervision: T.M.H., K.M., K.R.M., and J.J.D. Writing—original draft: K.L.B., R.A.P., K.D.M., K.R.M., C.E.N., and J.J.D. Writing—review and editing: K.L.B., R.A.P., E.T.J., C.E.N., M.T., K.M., T.M.H., L.I., M.E.Z., J.J.T., and J.J.D. **Competing interests:** The authors declare that they have no competing interests. **Data and materials availability:** All data needed to evaluate the conclusions in the paper are present in the paper and/or the Supplementary Materials and can also be found on Zenodo: https://doi.org/10.5281/zenodo.14207339. Custom code can be found at https://doi.org/10.5281/zenodo.14201265. Sequencing data that support the findings of this study are available in Gene Expression Omnibus. Accession numbers of specific datasets are as follows: bulk RNA-seq *Reln* CRISPRi, GSE269366; and snRNA-seq *Reln* CRISPRi, GSE269490.

Submitted 13 August 2024
Accepted 20 February 2025
Published 26 March 2025
10.1126/sciadv.ads4441